minerals

MDPI

Article

Environmental Controls on Maastrichtian Carbonate Platforms: Evidence from the Besni and Garzan Formations, SE Türkiye

Derya Sinanoğlu [1], Salih Dinç [2,*], Nazire Özgen-Erdem [3] and İsmail Ömer Yilmaz [4]

[1] Department of Petroleum and Natural Gas Engineering, Batman University, Bati Raman Campus, 72100 Batman, Türkiye; derya.sinanoglu@batman.edu.tr
[2] Department of Geological Engineering, Batman University, Bati Raman Campus, 72100 Batman, Türkiye
[3] Department of Geological Engineering, Cumhuriyet University, 58140 Sivas, Türkiye; nozgen@cumhuriyet.edu.tr
[4] Department of Geological Engineering, Middle East Technical University, 06800 Ankara, Türkiye; ioyilmaz@metu.edu.tr
* Correspondence: salih.dinc@batman.edu.tr

Abstract

This study correlates the Besni and Garzan formations, which are stratigraphically equivalent Maastrichtian (Late Cretaceous) carbonate platforms in the Southeastern Anatolia Region of Türkiye (Batman and Adıyaman). Situated along the northern margin of the Arabian Plate, this tectonically active region is highly critical as it hosts nearly 99% of the country's petroleum exploration and production activities. Although both formations consist of beige to yellowish, algae and benthic foraminifera-bearing limestones of the same age, integrated paleontological, petrographic, and geochemical evidence reveals that they developed under contrasting environmental conditions: The Besni Formation contains hyaline-calcareous *Orbitoides*, *Omphalocyclus*, *Siderolites* and the microgranular *Loftusia* larger benthic foraminifera in packstone, grainstone and wackestone facies, indicating a relatively high-energy shallow-marine setting. The Garzan Formation is dominated by porcelaneous, microgranular and agglutinated foraminifera and dasycladalean algae in packstone, indicating a relatively protected, lower-energy setting. Geochemically, SiO_2 contents range from 0.36 to 18.73 wt.% in the Besni Formation and 0.81 to 7.30 wt.% in the Garzan Formation, indicating the input of silica-rich detrital material during sedimentation. Positive $\delta^{13}C$ values in both formations are consistent with deposition in a shallow-marine environment. Ce/Ce* values (0.58–1.49 for Besni; 1.12–1.19 for Garzan) are close to unity, and together with positive correlations between ΣREE and detrital proxies (SiO_2, Al_2O_3, Fe), suggest detrital influence; they do not allow an unambiguous redox reconstruction. REE patterns are depleted relative to PAAS. In conclusion, despite their stratigraphic equivalence, the investigated sections of the two formations differ in depositional energy, as reflected mainly in their foraminiferal assemblages and microfacies, whereas their bulk geochemical signatures are broadly comparable.

Keywords: Besni formation; Garzan formation; stable isotope geochemistry; larger benthic foraminifera; carbonate sedimentology

Check for updates

Academic Editor: Olev Vinn

Received: 16 September 2026
Revised: 9 November 2026
Accepted: 21 November 2026
Published: 26 November 2026

Copyright: © 2026 by the authors. Licensee MDPI, Basel, Switzerland. This article is an open access article distributed under the terms and conditions of the Creative Commons Attribution (CC BY) license.

1. Introduction

The abundance and diversity of benthic foraminiferal species preceding the Cretaceous–Paleogene (K/Pg) boundary, the most recent major mass extinction event, are of fundamental importance for paleoenvironmental, paleoclimatic and paleogeographic reconstructions.

Cretaceous outcrops are widely distributed in Türkiye, as they are elsewhere around the world. Extensive carbonate deposition accompanied the widespread marine transgressions that occurred during the Cretaceous in the study area. The autochthonous Cretaceous succession of Southeastern Türkiye comprises numerous formations belonging to the Mardin and Şırnak groups. Perinçek et al. [1] assigned the Kastel, Bozova, Terbüzek, Besni, Haydarlı, Kıradağ, Garzan, Germav, Üçkiraz, Sinan, Antak, Kayaköy, Belveren and Becirman formations, deposited during the Late Campanian–Paleocene interval, to the Şırnak Group. The units comprising the group were deposited in a variety of depositional environments, ranging from terrestrial and transitional settings to shallow-marine and basinal environments [1,2]. The Şırnak Group succession, including the Besni and Garzan formations, exhibits a distinct paleogeographic differentiation from the Middle Maastrichtian onward, characterized by deeper-marine facies in the south and shallower-marine facies toward the north. In Southeastern Türkiye, stratigraphically equivalent units of the same age and lithology have been assigned different formation names by various authors, resulting in considerable stratigraphic nomenclatural inconsistency. Accordingly, the present study aims to compare the Besni and Garzan formations, which are regarded as stratigraphically equivalent on the basis of their age and lithological characteristics. The Besni and Garzan formations have so far largely been studied separately: stratigraphy, biostratigraphy and foraminiferal content for the Besni Formation, and foraminiferal assemblages and reservoir properties for the Garzan Formation [3]. The Garzan Formation constitutes an important hydrocarbon reservoir and therefore has considerable economic significance, whereas the Besni Formation does not possess comparable reservoir properties. Regional studies have correlated these units lithostratigraphically but have not compared their petrographic, paleontological and geochemical data together. Although both formations are conformably overlain by the Germav Formation, they differ in terms of their underlying stratigraphic units [2,3].

This study aims to investigate the foraminiferal assemblages of the Upper Cretaceous shallow-marine carbonates and to evaluate the stratigraphic evolution, biostratigraphy (with particular emphasis on larger benthic foraminiferal (LBF), biostratigraphy) and sedimentological characteristics of the shallow-marine successions in Southeastern Türkiye. Within the framework of benthic foraminiferal biostratigraphy, measured stratigraphic sections were established in the marine sedimentary successions of the study area, and the foraminiferal content of the carbonate rocks was systematically documented. Based on the identified foraminiferal taxa and biostratigraphic zones, the age and depositional environments of the investigated units were determined. Furthermore, this study aims to provide a comprehensive comparison of the Besni and Garzan formations through the integrated interpretation of paleontological, petrographic and geochemical data.

To our knowledge, this study presents the first integrated sedimentological, petrographic, paleontological and geochemical comparison of the Maastrichtian Besni and Garzan carbonate platforms and evaluates the environmental controls that may explain their contrasting larger benthic foraminiferal assemblages within the Northern Arabian Platform.

2. Stratigraphy of the Region

Seven measured stratigraphic sections were investigated in this study, including six sections from the Besni Formation in Adıyaman Province and one section from the only exposed outcrop of the Garzan Formation within the study area, located in Batman Province. The Batman–Adıyaman region has been extensively investigated by numerous researchers, who have focused on elucidating its tectonic evolution and depositional history [4–19]. The Precambrian–Paleozoic succession of Southeastern Türkiye consists predominantly of sedimentary units deposited from the Cambrian to the end of the Permian. The Mesozoic

succession begins with the Triassic and is composed mainly of carbonate rocks. In contrast, the Cenozoic succession comprises both siliciclastic and carbonate units, predominantly of marine origin, with locally developed continental deposits [2,3,20,21].

The Adıyaman Basin is situated within the Folded Belt, the southernmost tectono-orogenic unit of Türkiye, bordering the Syrian–Arabian Platform. In the study area and its vicinity, the basement is represented by the Koçali Complex, which is unconformably overlain by the autochthonous succession. The autochthonous units exposed in and around the study area comprise the Terbüzek, Besni, Germav, Gercüş, Midyat, and Gölbaşı formations, as well as Quaternary alluvial deposits. Located south of the Ecemiş–Karataş fault zone, the stratigraphic succession in the study area is tectonically overlain by allochthonous nappes (Upper Allochthonous Unit) [22].

In the Batman region of the study area, the stratigraphic succession begins with the Kıradağ Formation, which is not exposed at the surface, and continues upward with the Garzan Formation, deposited during a regional marine transgression and exposed in the core of the Gerçüş Anticline. The oldest unit exposed in the study area is the Garzan Formation of the Şırnak Group, which consists of beige to yellowish, algae and larger benthic foraminifera-bearing limestones. Continued deepening of the basin resulted in the conformable deposition of the Lower Germav Formation above these carbonates. This Upper Maastrichtian marine unit consists of light gray, fossiliferous carbonate siltstone, argillaceous limestone and marl interbeds. The Lower Germav Formation is conformably overlain by the Paleocene Upper Germav Formation, which is composed predominantly of dark gray marl together with greenish-gray sandstone and mudstone. Upsection, the Upper Germav Formation exhibits a regressive trend, grading into limestone and sandstone. The stratigraphic succession culminates in the deposition of the entirely continental Antak Formation following the final regression. The Paleocene Antak Formation, a fluvial unit composed of conglomerate, sandstone, and mudstone, together with the coeval strata, has been assigned to the Şırnak Group. Subsequently, a Middle Eocene marine transgression led to the deposition of the shallow-marine limestones of the Hoya Formation. The Hoya Formation unconformably overlies the Şırnak Group across an angular unconformity and has been assigned to the Midyat Group. In the study area, the Eocene succession is represented exclusively by the carbonate rocks of the Hoya Formation [3,20,21].

2.1. Besni Formation

The Besni Formation was first defined by Krummenacher and Periam [23] in the vicinity of Besni, Adıyaman Province. The formation is exposed as a relatively narrow belt along the northern part of the basin, immediately in front of the allochthonous units. Its southern limit is marked by a line extending from southern Adıyaman through northern Kahta to Karadağ.

In the Adıyaman region, the Besni Formation is exposed around Taşyazı, Besni, Palanlı, Dumlu, and Alidam (Figures 1 and 2A,B). In the vicinity of Toybelen Village to the north of Adıyaman and Taşlıyazı Village to the west, the formation is represented predominantly by light beige to cream-colored, generally biosparitic limestones. At its exposed localities, the formation begins with a basal interval, a few meters thick, consisting of yellow, soft, weathered sandstone overlain by light beige limestone containing ophiolitic sand- and gravel-sized clasts [5,11,24–33].

These basal beds contain abundant larger benthic foraminifera and shell fragments. Upsection, the succession grades into gray, yellow, and dirty white, hard to moderately hard, medium- to thick-bedded grainstone limestones containing abundant larger benthic foraminifera (*Loftusia*, *Orbitoides* and *Omphalocyclus*), together with molluscan, rudist, algal, and coral skeletal fragments (Figure 2C–F). Based on its facies characteristics, the Besni

Formation is interpreted to have been deposited in a high-energy shallow-marine environment. In the vicinity of Taşlıyazı Village (Adıyaman Province) and Karadut Village (Kahta District), the Besni Formation unconformably overlies the Terbüzek Formation [11,26,32]. Across the central and eastern parts of its outcrop area, it is conformably and gradationally overlain by the Lower Germav Formation. In the western and northwestern sectors, the Besni Formation is unconformably overlain by the Upper Germav or Belveren formations [13].

The Besni Formation is 15–35 m thick at its type section near Besni. In the study area, the layer thickness of the formation varies between 32 and 63 m (Table 1). Based on previous studies, the formation has been assigned a Middle–Late Maastrichtian age [11,34–36] (Figures 1 and 2). Examination of samples collected from the measured stratigraphic section revealed the occurrence of characteristic Maastrichtian larger benthic foraminifera and associated benthic taxa, including *Loftusia kahtaensis* Meriç, *Orbitoides medius* (d'Archiac), *Omphalocyclus macroporus* (Lamarck), *Lenticulina rotulata* Lamarck, *Sirtina ornata* Rahaghi, *Fissoelphidium operculiferum* Smout, *Elazigina siderea* Consorti and Rashidi, *Siderolites calcitropoides* Lamarck, *Stomatorbina* sp., *Goupilloidina* sp., *Kolchidina* sp., *Valvulineria* sp., *Orbitoides* sp., and *Hadonnia* sp., supporting a Maastrichtian age for the formation.

Table 1. Thickness, lithology, fossil content, and vertical variation of the Besni and Garzan formations.

Section	Thickness (m)	Lithology and Color	Bedding/Bed Thickness	Fossil Content and Structures	Vertical Variation
BS1	**32**	Yellow, off-white in color	Medium-to-thick bedded, massive-appearing	Fractured, containing large benthic foraminifera (orbitoidal forms, *Loftusia*, and rudist shells)	Bottom-to-top packstone
BS2	**33**	Yellow, off-white in color	Medium-to-thick bedded, massive-appearing	Fractured, containing large benthic foraminifera (orbitoidal forms, *Loftusia Siderolites*, and rudist shells)	Bottom-to-top packstone
BS3	**63**	Light yellow, beige in color	Well-bedded	Fractured, broken; rich in orbitoidal and miliolidal forms, *Loftusia*, and rudist shells	Sandy limestone → grainstone/packstone
BS4	**62**	Light yellow, beige in color	Medium-to-thick bedded	Fractured, containing large benthic foraminifera (orbitoidal forms, *Loftusia*, and rudist shells)	Sandy Dolomitic Limestone → Sandy limestone → packstone
BS5	**33**	Light yellow, beige in color	Medium-to-thick bedded	Fractured, containing large benthic foraminifera (orbitoidal forms, abundant *Loftusia* and *Siderolites*)	Sandy Dolomitic Limestone → Sandy limestone → packstone
BS6	**42**	Light yellow, beige in color	Medium-to-thick bedded	Fractured, containing large benthic foraminifera and algae (orbitoidal forms, abundant *Loftusia* and *Siderolites*)	Wackestone → dolomitic limestone → sandy limestone → packstone
GA	**126**	White, cream, gray in color	Well-bedded to massive at the base, nodular in the middle	Dissolution voids, fractures, asphaltite (*Discyclina*, *Antalyna*, *orbitoid* forms, and abundant shell fragments)	Upward-increasing clay, transition to Germav

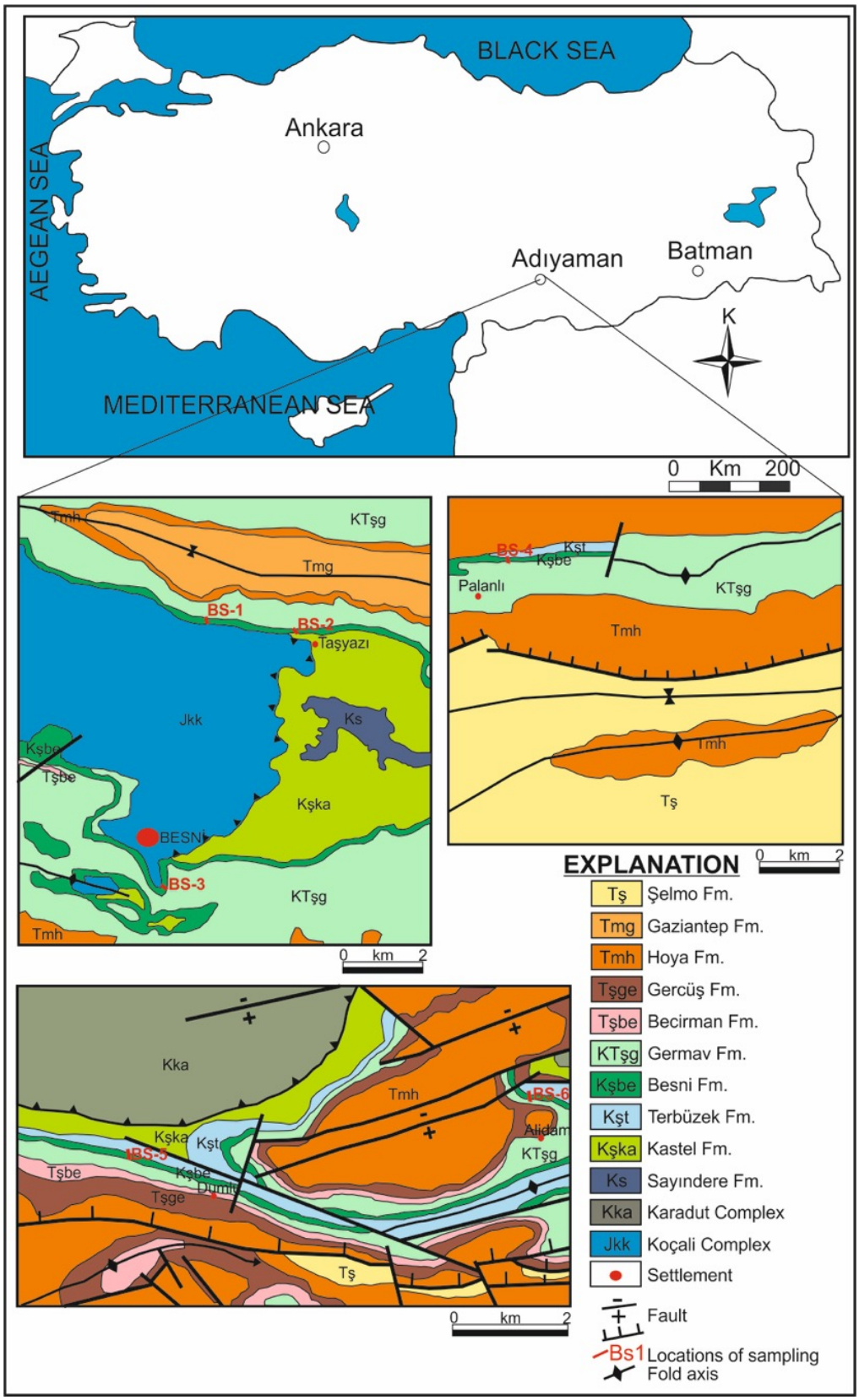

Figure 1. Geological map of the study area and locations of sampling (BS1–BS6). Prepared using [25–28,37,38].



Figure 2. Field views of the contact between the Besni and Germav formations (**A**) and between the Terbüzek and Besni formations (**B**). Views of *Acteonella* sp. within the carbonates of the Besni formation (**C**–**F**).

2.2. Garzan Formation

The Garzan Formation, which constitutes one of the principal reservoir units of the Garzan Oil Field and derives its name from the Garzan (Yanarsu) Stream flowing south of the field, was first defined by Kellogg [39]. Composed predominantly of shallow-marine limestones, the formation was deposited over a wide area and serves as a productive hydrocarbon reservoir in numerous oil fields [3,19]. It is widely regarded as the lateral equivalent of the Besni Formation to the west and the Üçkiraz Formation, defined in the Hakkari region and extending into the eastern part of the study area [13]. In the study area, the Garzan Formation forms a broad topographic high owing to its greater resistance to erosion relative to the surrounding shales of the Germav Formation (Figure 3). Its principal lithology consists of bioclastic limestones containing porcelaneous, microgranular and agglutinated benthic foraminifera and dasycladalean algae [3,19]. Thin intercalations of argillaceous limestone and marl are locally present within the formation. The unit is characterized by white, cream, gray, light gray, and beige colors, and consists of hard to very hard limestones displaying distinct but locally discontinuous bedding, ranging from

thin-bedded to massive [3,19]. It is highly fossiliferous and commonly exhibits abundant fractures and dissolution cavities. Asphaltite and heavy oil residues are locally observed in the upper part of the formation (Figure 4A–D).

Across the basin, the Garzan Formation is 150–200 m thick, whereas a thickness of approximately 126 m has been measured in the stratigraphic section west of Gerçüş (Table 1). The basal contact of the Garzan Formation is not exposed in the study area (Figure 3). Data from wells drilled by the Turkish Petroleum Corporation (TPAO) indicate that the formation overlies the siliciclastic Kıradağ Formation [20,21]. Although the Kıradağ Formation has been interpreted as representing the basal clastic unit associated with the Maastrichtian marine transgression, it has also been suggested that its contact with the Garzan Formation is unconformable [13,40]. However, Özer et al. [41] proposed that the Maastrichtian units (Terbüzek, Besni, Kıradağ, Garzan, Üçkiraz, and Germav formations) are laterally and vertically transitional throughout the Zagros Belt.

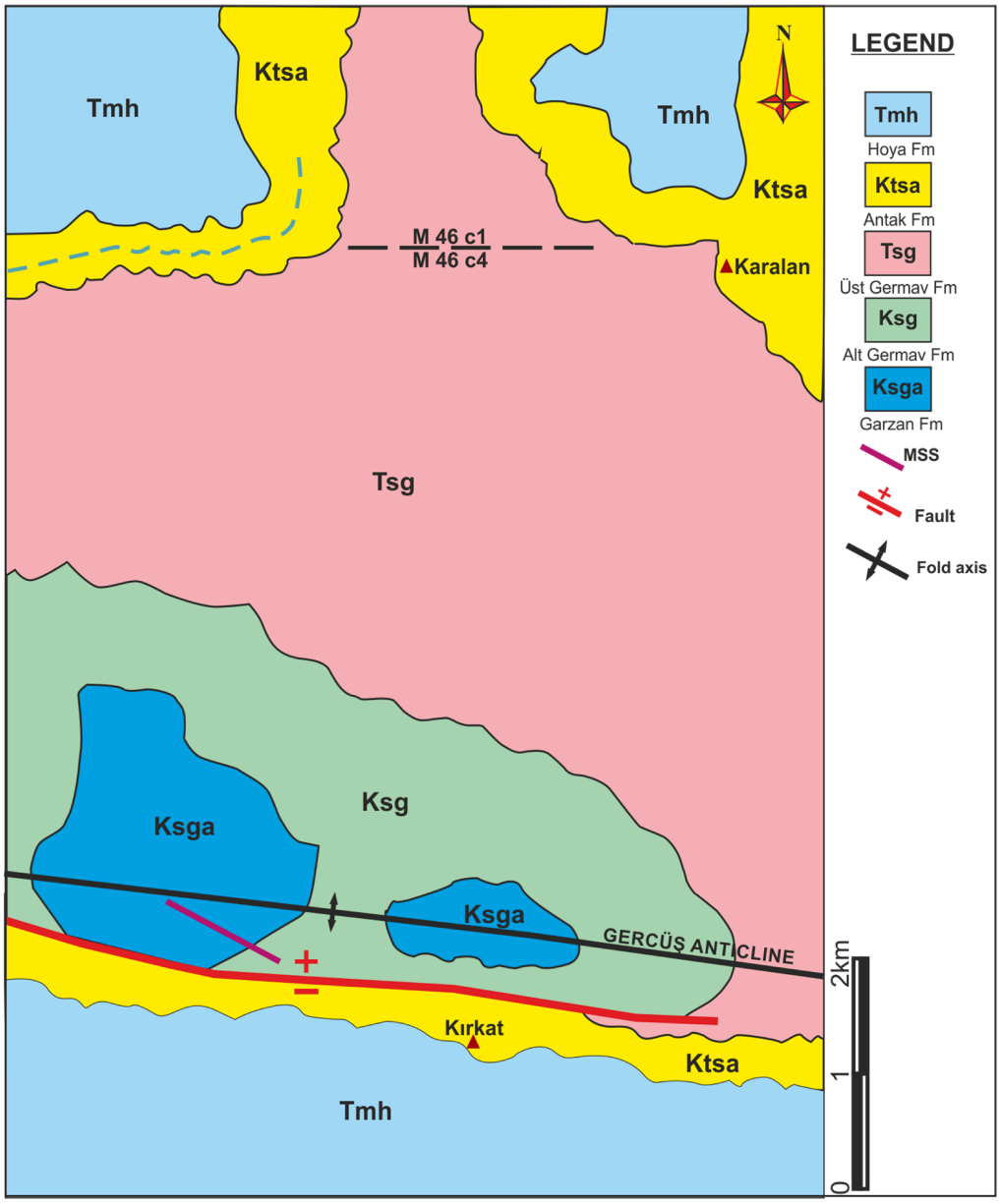

Figure 3. Location map and geological map of the study area (Kırkat). Modified after [20].

Accordingly, considering that a basal siliciclastic interval is commonly developed at the onset of marine transgressions, the Kıradağ and Terbüzek formations may also be laterally and vertically transitional with the Garzan, Besni and Üçkiraz formations. In the core of the Gerçüş Anticline, the Garzan limestones, which exhibit a progressive increase in clay content upward, grade conformably into the Germav Formation [3,19]. Samples collected from the measured stratigraphic section yielded a characteristic Maastrichtian assemblage comprising *Orbitoides megaloformis* Papp ve Küpper, *Orbitoides medius* (d'Archiac), *Siphopfenderina geyikensis* (Solak), *Fleuryana adriatica* (De Castro), *Sirtina orbitoidiformis* Brönnimann and Wirtz, *Trochospira avnimelechi* Hamaoui, *Cuneolina ketini* İnan, *Dicyclina schlumbergeri* Munier-Chalmas, *Vandenbroekia munieri* Marie, *Nezzazatinella picardi* (Henson), *Monsharmontia apenninica* (De Castro), *Dictyoconella complanata* Henson, *Antalyna korayi* Farinacci and Köylüoğlu, *Pseudomphalocyclus blumenthali* Meriç, and *Omphalocyclus* sp. together with representatives of the rotaliid, miliolid, and textulariid benthic foraminiferal groups. In addition, macrofossils including corals, echinoderms, molluscs, ostracods, rudists, and dasycladalean green algae were identified.

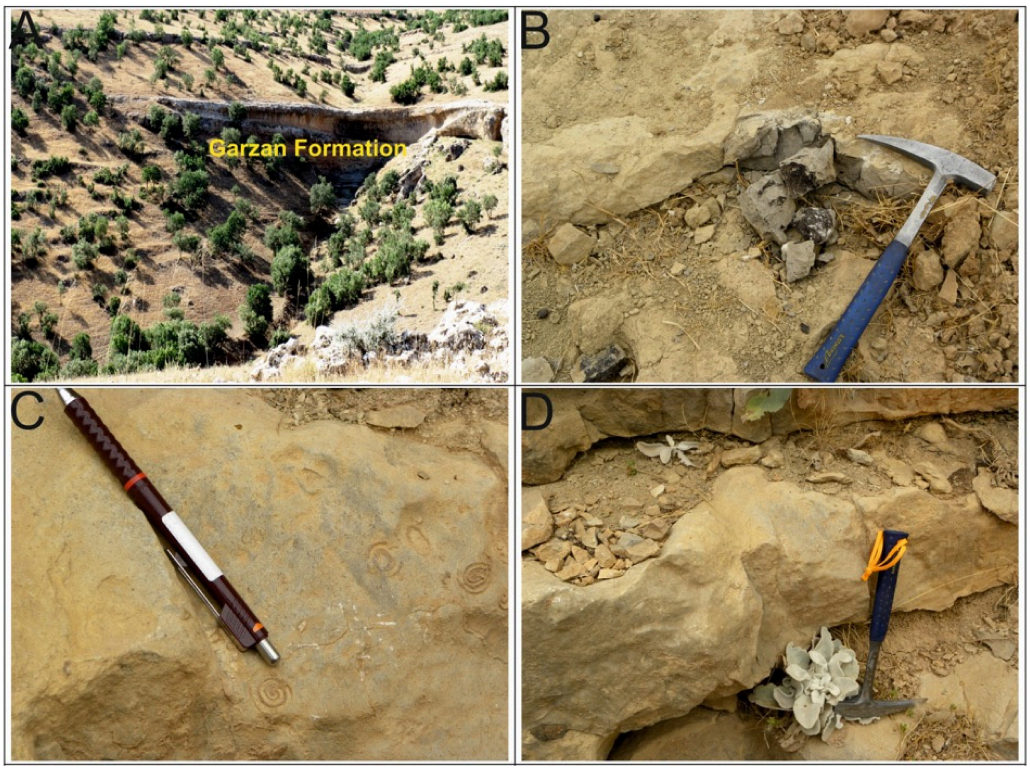

Figure 4. (**A**) The only outcrop belonging to Garzan Fm around Gercüş Fm. (**B**) Asphaltite residue in the Garzan formation. (**C**) Macrofossil fragment. (**D**) View of the stratification in the Garzan formation.

3. Materials and Methods

Samples were collected from the Besni Formation exposed around Taşyazı, Besni, Palanlı, Dumlu, and Alidam in Adıyaman Province, and from the Garzan Formation exposed near Gerçüş in Batman Province (Figure 1). A total of 61 thin sections of carbonate rocks were prepared and examined petrographically: 46 from the Besni Formation (BS1 = 4, BS2 = 7, BS3 = 10, BS4 = 14, BS5 = 3, BS6 = 8) and 15 from the Garzan Formation (section GA). The relative percentages of bioclasts, intraclasts, sparite, and micrite were estimated by visual examination of the prepared thin sections under a polarizing microscope, and the samples were texturally characterized in accordance with the Dunham [42] carbonate

classification scheme. These include sandy limestones, in which detrital quartz and other non-carbonate grains occur in a carbonate matrix; no siliciclastic (sandstone) thin sections were examined. The oriented sections were obtained by identifying suitable larger benthic foraminiferal tests in the prepared thin sections and selecting the cutting direction according to the visible morphology and orientation of each test. Where preservation permitted, equatorial and axial sections were examined to document the internal test architecture. Thin sections of lithified rock samples were prepared at the Thin Section Laboratory of the Department of Geological Engineering, Sivas Cumhuriyet University. Petrographic analyses were carried out using a Leica DP2500 polarizing microscope (Leica Microsystems GmbH, Wetzlar, Germany) at the Microscopy Laboratory of the Department of Geological Engineering, Batman University. During petrographic examination, the Alizarin Red S staining technique was employed to distinguish calcite from dolomite. A few drops of hydrochloric acid-diluted Alizarin Red S solution were applied to the thin sections, resulting in calcite being stained red, whereas dolomite exhibited no color change.

Oriented thin sections of larger benthic foraminifera were also prepared at the Thin Section and Paleontological Research Laboratory of the Department of Geological Engineering, Sivas Cumhuriyet University. Equatorial sections are particularly critical for the taxonomic identification of larger benthic foraminifera such as *Orbitoides*, *Omphalocyclus* and *Loftusia*.

Petrographic examination of the thin sections was undertaken to determine the calcite and dolomite contents of the carbonate rocks. Based on the petrographic results, fifteen representative samples were selected for whole-rock geochemical analyses. Major oxide, trace element, and rare earth element (REE) analyses were performed at ACME Analytical Laboratories Ltd. (Vancouver, BC, Canada inductively coupled plasma-based analytical techniques.

Major and trace element analyses of the carbonate samples were carried out at ACME Analytical Laboratories Ltd. (Vancouver, BC, Canada). The major elemental compositions of fifteen selected carbonate samples were determined using inductively coupled plasma mass spectrometry (ICP-MS). The standard LF300 analytical package was employed for major oxide determinations. Throughout the whole-rock major element analyses, the certified reference material STD SO-19 was used for quality control.

Stable carbon and oxygen isotope ($\delta^{13}C$ and $\delta^{18}O$) analyses were performed on 24 carbonate samples at the Central Laboratory, Research and Development, Education and Measurement Center of Middle East Technical University (METU). The $\delta^{13}C$ and $\delta^{18}O$ isotope ratios of the carbonate samples were determined using a GasBench II (Thermo Fisher Scientific, Bremen, Germany) continuous-flow isotope ratio mass spectrometry (CF-IRMS) system coupled to a DeltaPlus XP Isotope Ratio Mass Spectrometer (Thermo Finnigan, Bremen, Germany).

$\delta^{13}C$ and $\delta^{18}O$ isotope analyses of the carbonate samples were conducted at the Stable Isotope Laboratories of Middle East Technical University (METU-Ankara). Powder samples weighing approximately 2–10 mg were obtained from the limestones using a micromill drilling technique. A GasBench II continuous-flow isotope ratio mass spectrometer coupled to a DeltaPlus XP mass spectrometer (Thermo Finnigan, Bremen, Germany) was used.

Carbonate samples of 0.2–0.4 mg were weighed on a precision balance and placed in sample wells. Each sample was allowed to react with Ortho-Phosphoric acid 99% (MERCK) (about 0.1 mL) for a period (about two hours) in an autosampler tray maintained at about 70 °C. The CO_2 gas produced by this reaction is sent to the mass spectrometer to be separated into isotopes after purification by the Gas Bench interface. The ion ratios of CO_2 were converted into raw isotopic ratios using ISODAT 2.0. software. In the analysis, the standard "NBS19 Limestone (NIST)" (δ13C: 1.95‰ and δ18O: −2.20‰) as the main

standard was analyzed in each experiment set and used to convert the raw isotope ratios of the samples determined by the device to true isotopic values. The results are determined in terms of permil VP according to VPDB (Vienna Pee Dee Belemnite). The 1σ error margins for the δ13C and δ18O isotope ratios do not exceed 0.2‰. All analyzed samples are stored in the Paleontology Laboratory of the Department of Geological Engineering at Sivas Cumhuriyet University.

The Garzan Formation crops out at only one locality in the study area, and its other parts are accessible only through drilling; therefore, six measured sections were established in the Besni Formation but only one in the Garzan Formation. Whole-rock geochemical analyses were limited to 15 samples (12 Besni, 3 Garzan). The geochemical comparison is thus based on a limited and uneven dataset, and the Garzan results in particular may not capture the full lateral variability of the formation across the basin. The interpretations presented here therefore refer to the investigated sections rather than to the formations at the regional scale.

4. Results

4.1. Petrography of Carbonate Rocks—Besni Formation

To determine the mineralogical and petrographic characteristics of the carbonate rocks of the Besni Formation, six measured stratigraphic sections (BS1–BS6) were established at different outcrop localities. The locations of these measured sections are shown in Figure 5.

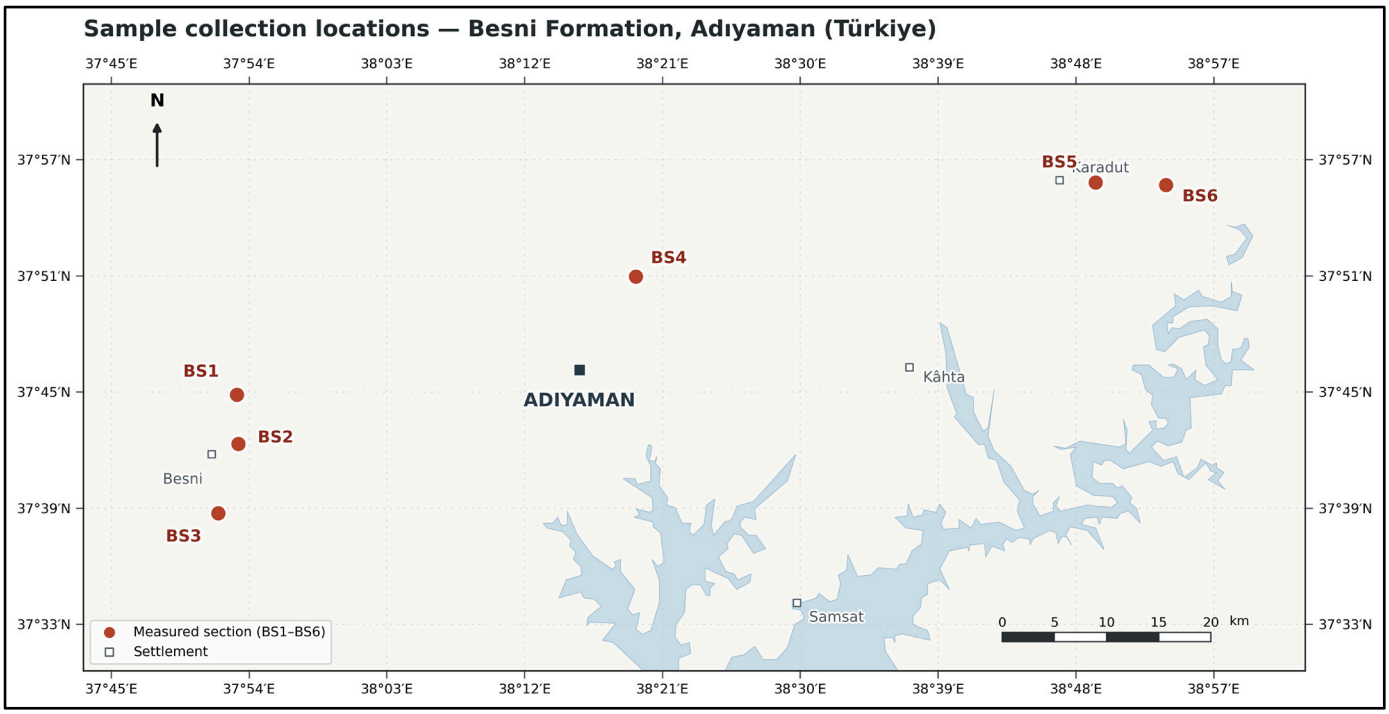

Figure 5. Sample collection locations in Adıyaman Province (Taşyazı, Besni, Palanlı, Dumlu, and Alidam).

Lithological variations within the Besni Formation were determined based on the petrographic characteristics of samples collected from the measured stratigraphic sections. Carbonates from the BS1 and BS2 sections are composed predominantly of packstone ([42], Tables 1 and 2). The BS1 and BS2 samples are grain-supported, with 65%–82% bioclasts and 5%–35% micritic matrix (Table 2). In the BS3 section, the carbonate succession begins with sandy limestone at the base, passes upward into alternating grainstone and packstone, and grades into packstone in the upper part of the section. Carbonates in the BS4 and BS5

sections commence with sandy dolomitic limestone at the base, followed upward by sandy limestone, and finally grade into packstone. In the BS6 section, the carbonate succession begins with wackestone at the base and passes upward into dolomitic limestone, sandy limestone, and packstone (Tables 1 and 2). Correlation of the lithological data obtained from the measured stratigraphic sections is presented in Figure 6. Petrographic examination of thin sections prepared from 46 carbonate rock samples collected from the measured stratigraphic sections revealed minor porosity together with trace amounts of muscovite, biotite, and other accessory minerals. Fractures are commonly filled with calcite and locally coated with iron oxide.

Table 2. Microscopic characteristics of samples taken from BS1–BS6 (Besni Formation; Q: Quartz, dm: Other minerals).

Sample No.	Calcite Content %	Dolomite Content %	Rock Particles/ Other Minerals	Allochems			Ortochems		Rock Name [42]
				Fossils %	İntraclast %	Ooid %	Pellet %	Sparite %	Micrite %	
BS1-1	95	-	5	70	-	-	-	17	8	Packstone
BS1-2	100	-	-	82	-	-	-	3	15	Packstone
BS1-3	100	-	-	79	-	-	-	8	13	Packstone
BS1-4	100	-	-	80	-	-	-	5	15	Packstone
BS2-1	100	-	-	75	-	-	-	10	15	Packstone
BS2-2	100	-	-	73	3	-	-	15	9	Packstone
BS2-3	100	-	-	80	-	-	-	10	10	Packstone
BS2-4	100	-	-	77	1	-	-	7	15	Packstone
BS2-5	100	-	-	68	-	-	-	2	30	Packstone
BS2-6	100	-	-	65	-	-	-	-	35	Packstone
BS2-7	100	-	-	67	5	-	1	12	15	Packstone
BS3-1	85	-	15 (Q)	45	20	-	-	-	20	Sandy Limestone
BS3-2	85	-	15 (Q + dm)	42	20	-	-	15	8	Sandy Limestone
BS3-3	100	-	-	78	1	-	-	20	1	Grainstone
BS3-4	100	-	-	-	77	-	-	20	3	Grainstone
BS3-5	100	-	-	80	-	-	-	20	-	Grainstone
BS3-7	100	-	-	79	-	-	1	2	18	Packstone
BS3-8	100	-	-	80	1	-	-	5	14	Packstone
BS3-9	100	-	-	78	-	-	-	20	2	Grainstone
BS3-10	100	-	-	73	-	-	-	2	25	Packstone
BS3-11	100	-	-	68	7	-	-	25	-	Grainstone
BS4-1	60	20	20 (Q + dm)	38	-	-	-	20	2	Sandy Dolomitic Limestone
BS4-2	90	-	10 (Q)	63	-	-	2	20	5	Sandy Limestone
BS4-3	80	-	20 (Q + dm)	38	20	-	-	20	2	Sandy Limestone
BS4-4	100	-	-	80	-	-	-	5	15	Packstone
BS4-5	100	-	-	78	-	-	-	2	20	Packstone
BS4-6	100	-	-	79	-	-	-	3	18	Packstone
BS4-7	100	-	-	80	-	-	-	2	18	Packstone
BS4-8	100	-	-	78	-	-	-	2	20	Packstone
BS4-9	100	-	-	68	-	-	-	2	30	Packstone
BS4-10	100		-	79	-	-	-	3	18	Packstone
BS4-11	100		-	78	-	-	-	15	7	Packstone
BS4-12	100		-	75	-	-	-	5	20	Packstone

Table 2. *Cont.*

Sample No.	Calcite Content %	Dolomite Content %	Rock Particles/ Other Minerals	Allochems			Ortochems		Rock Name [42]
				Fossils %	İntraclast %	Ooid %	Pellet %	Sparite %	Micrite %	
BS4-13	100		-	65	-	-	-	10	25	Packstone
BS4-14	100		-	78	-	-	-	2	20	Packstone
BS5-1	70	15	15 (Q + dm)	45	-	-	-	10	15	Sandy Dolomitic Limestone
BS5-2	100	-	20 (Q + dm)	65	-	-	-	5	10	Sandy Limestone
BS5-3	100	-	-	83	-	-	-	2	15	Packstone
BS6-1	93	7	30 (Algae)	10	18	-	-	10	25	Wackestone
BS6-2	100	-		-	20	-	-	80	-	Wackestone
BS6-3	70	30	40 (Algae)		-	-	-	10	20	Dolomitic Limestone
BS6-4	60	-	40 (Q + dm)	2	5	-	-	38	15	Sandy Limestone
BS6-5	95	-	5	65	-	-	-	15	15	Packstone
BS6-6	100	-	3	72	-	-	-	5	20	Packstone
BS6-7	100	-	-	77	-	-	-	3	20	Packstone
BS6-8	98	-	2	78	-	-	-		20	Packstone

Based on petrographic observations, the 46 carbonate rock samples were classified [42]. Of these, 30 samples were identified as packstone, five as grainstone, two as wackestone, six as sandy limestone, two as sandy dolomitic limestone, and one as dolomitic limestone (Table 2). The limestones contain abundant fossils, skeletal fragments, and intraclasts, together with minor amounts of peloids, whereas sparry calcite and micrite constitute the principal cement and matrix components. The proportions of allochems and orthochems range from 2%–83% fossils, 1%–77% intraclasts, 1%–2% peloids, 2%–80% sparry calcite, and 1%–68% micrite (Figure 7A,B,D–F). Dolomite crystals in the carbonate rocks are fine- to medium-crystalline, anhedral, xenotopic, and characterized by irregular crystal boundaries. Fine- to medium-crystalline calcite locally occurs between dolomite crystals (Figure 7C). In addition to carbonate minerals, some thin sections contain non-carbonate minerals, including quartz, which locally constitutes up to 15% of the rock (Figure 7E,F). In this strictly descriptive petrographic context, these detrital quartz-bearing intervals characterized by sub-angular to sub-rounded terrigenous siliciclastic grains within the micritic or sparry matrix are classified as sandy limestones, indicating proximity to terrigenous influx zones.

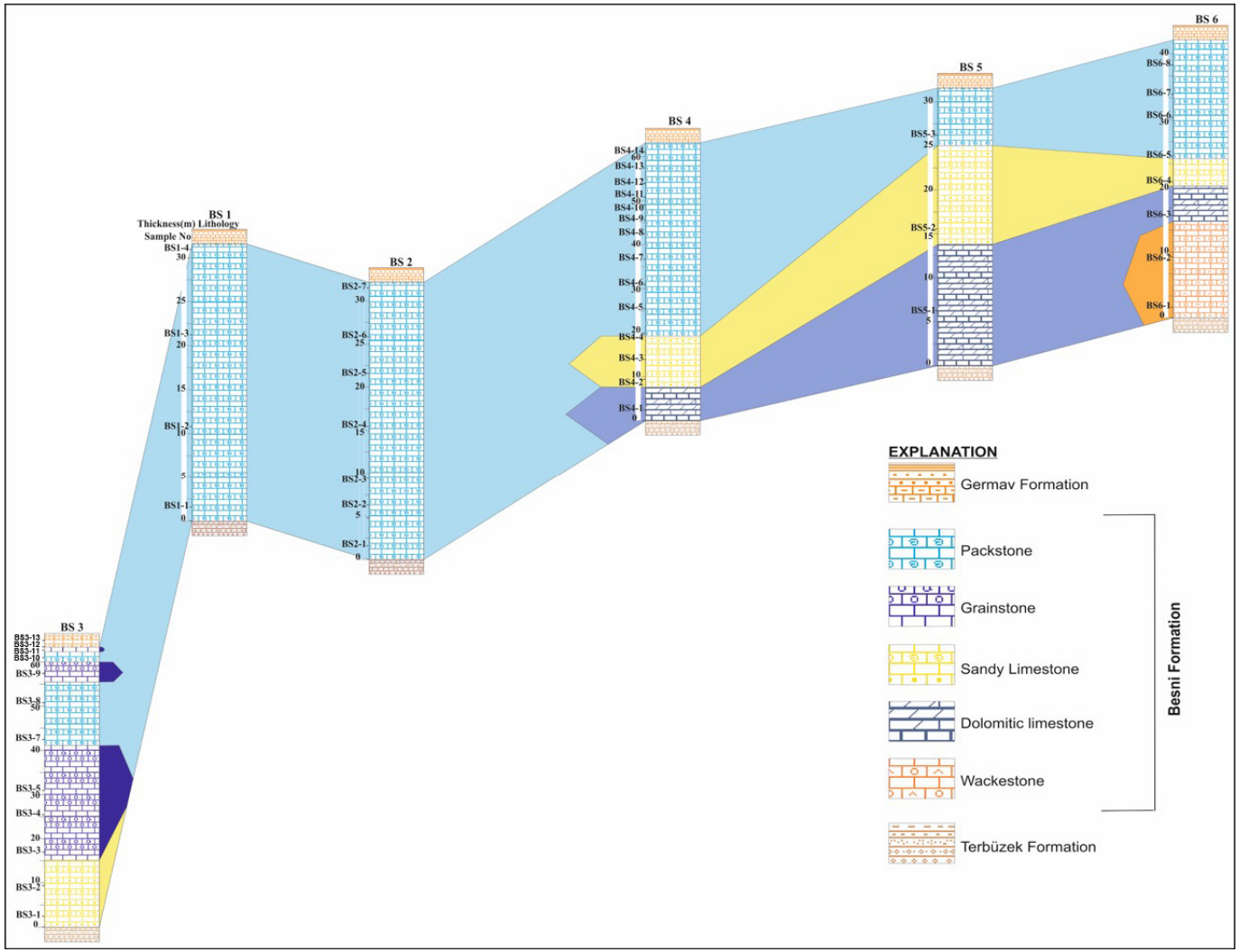

Figure 6. Lithostratigraphic correlation of the measured stratigraphic sections (BS1–BS6) of the Besni Formation. The datum is the contact between the Besni and Germav formations. Correlation polygons between sections are interpolated and do not represent time lines. Sample numbers and thicknesses (m) are shown along each column. MSS, measured stratigraphic section.

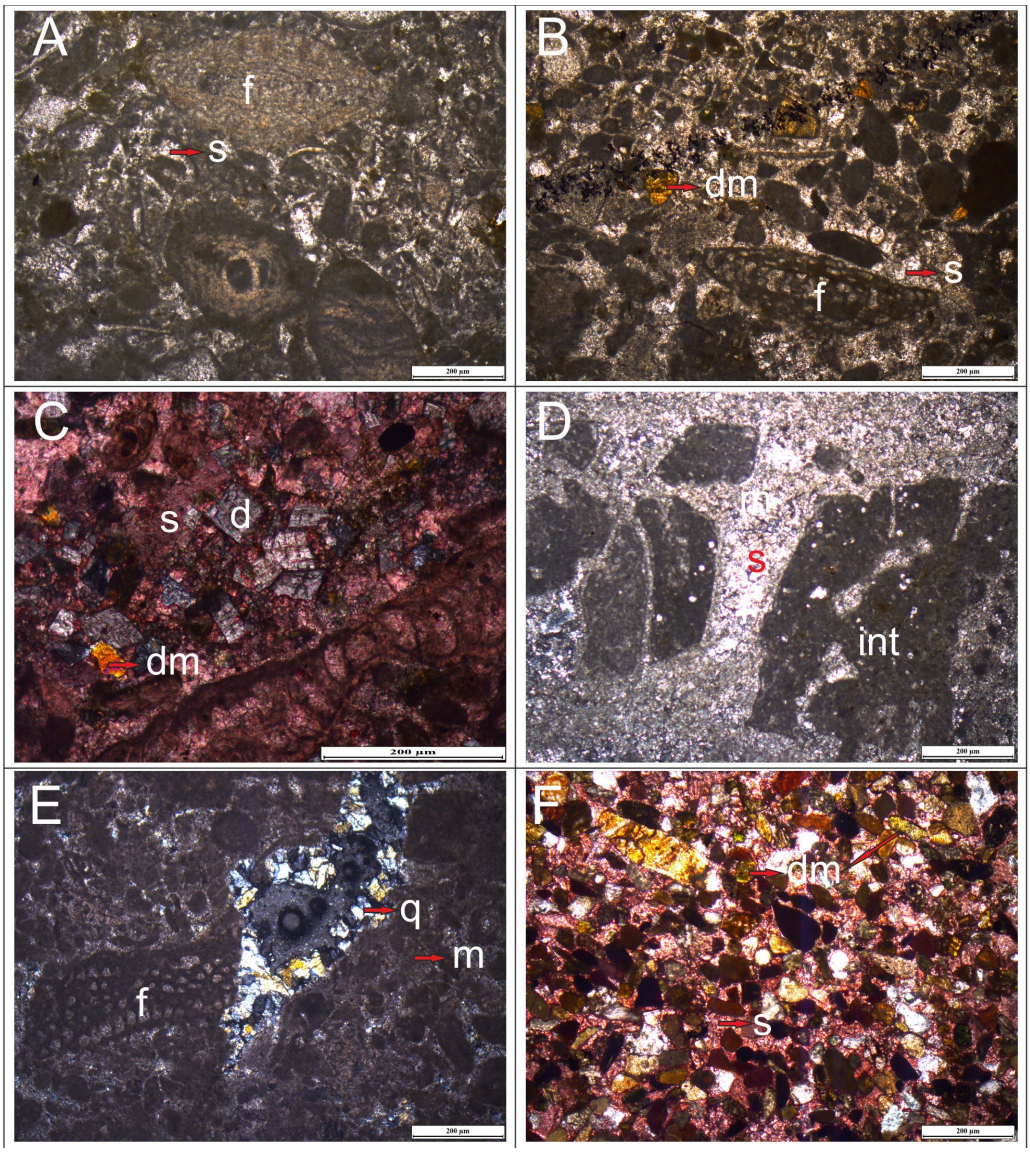

Figure 7. Photomicrographs of carbonate rocks of the Besni Formation. (**A**) Bioclastic packstone with larger benthic foraminifera (f) in a micritic matrix and sparry calcite (s) [PPL]. (**B**) Sandy limestone with bioclasts (f), sparite (s) and non-carbonate grains (dm) [PPL]. (**C**) Dolomitic limestone stained with Alizarin Red S; dolomite (d) is unstained and calcite is stained red [XPL]. (**D**) Wackestone with intraclasts (int) cemented by sparite (s) [PPL]. (**E**) Sandy limestone with quartz (q) and a foraminiferal fragment (f) in micrite (m) [XPL]. (**F**) Sandy limestone with detrital grains and other minerals (dm) in sparite (s) [XPL]. Abbreviations: f, fossil; m, micrite; s, sparite; d, dolomite; int, intraclast; q, quartz; dm, other minerals. Scale bars: 200 µm.

4.2. Petrography of Carbonate Rocks—Garzan Formation

To determine the mineralogical and petrographic characteristics of the carbonate rocks of the Garzan Formation, a measured stratigraphic section (GA) was established in the study area near Gerçüş, and 15 carbonate rock samples were collected. Lithological variations within the Garzan Formation were evaluated based on the petrographic characteristics of samples obtained from the measured stratigraphic section. Petrographic examination of thin sections prepared from the 15 carbonate rock samples revealed only minor porosity. Fractures are commonly filled with calcite and locally coated with iron oxides. Based on the petrographic observations, all 15 carbonate rock samples were classified as packstone ([42], Table 3). The limestones contain abundant fossils and skeletal fragments, together with minor amounts of peloids. Sparry calcite and micrite constitute the principal cement and

matrix components. The allochemal and orthochemical constituents comprise 55%–95% fossils, 2%–3% peloids, 2%–5% algae fragments, 7%–13% sparry calcite, and 5%–30% micrite (Figure 8A–H).

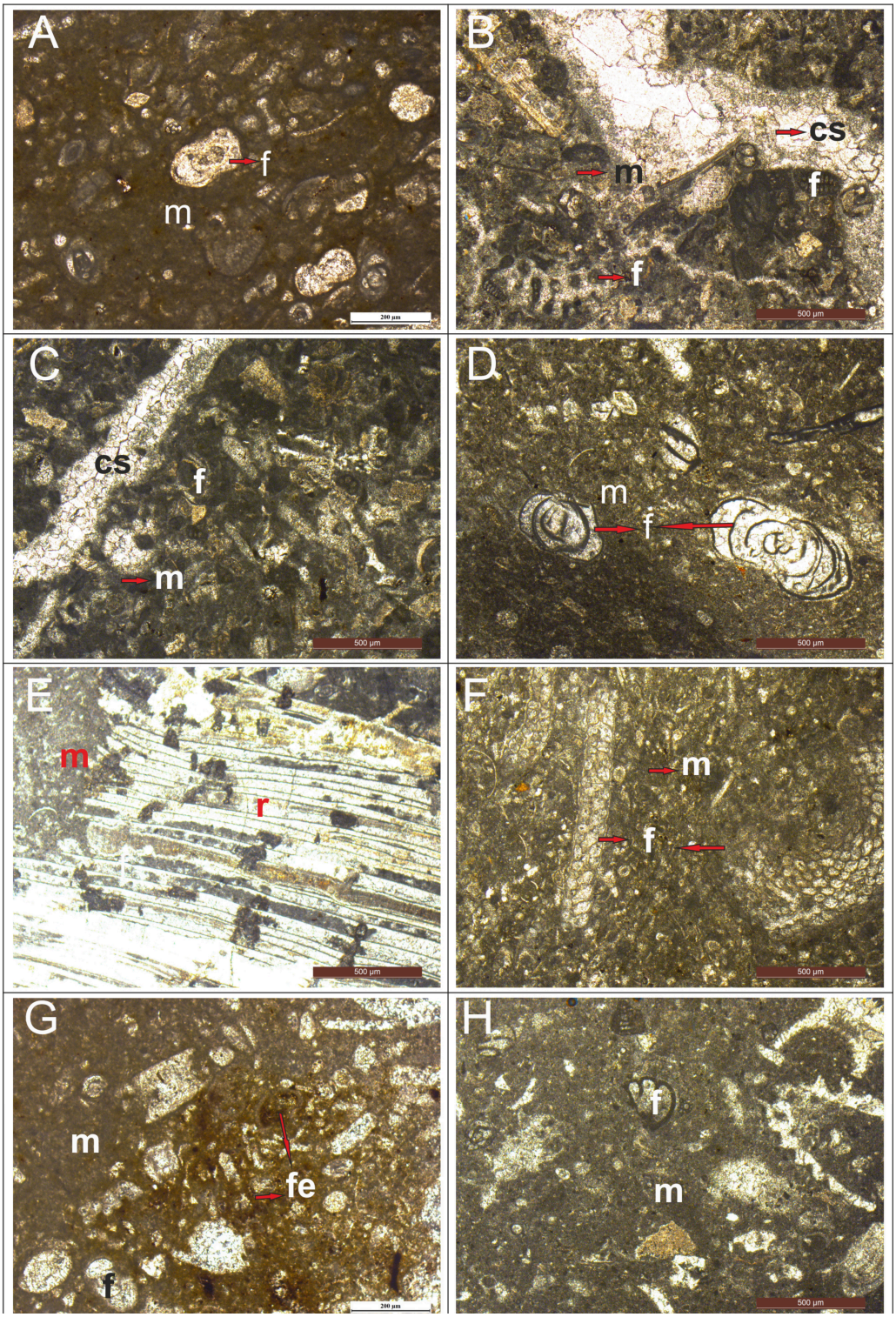

Figure 8. Photomicrographs of carbonate rocks of the Garzan Formation (all packstone). (**A**) Foraminifera (f) in a micritic matrix (m). (**B**,**C**) Fossil fragments (f) and micrite (m) cut by a sparite-filled fracture (cs). (**D**) Large benthic foraminifera (f) in micrite (m). (**E**) Rudist shell fragments (r) in a sparitic/micritic matrix. (**F**) Dasycladalean algae and foraminifera (f) in micrite (m). (**G**) Bioclasts (f), micrite (m) and iron oxide (fe). (**H**) Foraminifera (f) in micrite (m). Scale bars: 200 µm (A and G)/500 µm (**B**–**F**,**H**) per panel.

Table 3. Microscopic properties of samples taken from the Garzan Formation.

Sample No.	Calcite Content %	Dolomite Content %	Rock Particles/ Other Minerals	Allochems				Ortochems		Rock Name [42]
				Fossils %	İntraclast %	Ooid %	Pellet %	Sparite %	Micrite %	
GA-1	100	-	-	71				7	22	Packstone
GA-2	100	-	-	64				13	23	Packstone
GA-3	100	-	2 (Algae)	75				3	20	Packstone
GA-4	100	-	-	70	-	-	-	13	17	Packstone
GA-5	100	-	-	65					35	Packstone
GA-7	100	-	5 (Algae)	57				3	35	Packstone
GA-9	100	-	-	78					22	Packstone
GA-10	100	-	-	55	-	-	2	15	28	Packstone
GA-11	100	-	-	70			3		27	Packstone
GA-14	100	-	-	81				7	12	Packstone
GA-15	100	-	-	72				8	20	Packstone
GA-16	100	-	-	80			2		18	Packstone
GA-17	100	-	-	87					13	Packstone
GA-18	100	-	-	95					5	Packstone
GA-20	100	-	-	70	-	-	-	-	30	Packstone

4.3. Major Elements Geochemistry

The major oxide compositions of the Besni and Garzan formation samples are presented in Table 4. Several carbonate rock samples exhibited relatively high SiO_2 contents (3.07–18.73 wt.%), and were therefore classified as sandy (siliceous) limestone and sandy dolomitic limestone based on their petrographic and geochemical characteristics (Tables 2 and 4).

Table 4. Major (%), trace (ppm) and rare-earth elements concentration of samples from the Besni and Garzan formations.

Sample No. % and ppm	BS1-1	BS1-2	BS2-3	BS2-6	BS3-1	BS3-3	BS4-1	BS4-7	BS5-1	BS5-3	BS6-1	BS6-3	GA-4	GA-10	GA-20
SiO_2%	4.55	1.04	0.36	0.44	15.00	0.67	7.97	0.38	18.73	3.07	2.09	4.24	7.30	0.81	1.55
Al_2O_3%	0.46	0.28	0.08	0.02	0.73	0.16	0.96	0.07	3.51	0.83	0.48	0.97	0.93	0.09	0.27
Fe_2O_3%	0.64	0.32	0.20	0.09	0.77	0.33	1.73	0.11	2.23	0.70	0.41	0.95	0.49	0.05	0.51
MgO %	0.38	0.32	0.28	0.23	2.08	0.56	5.97	0.41	3.67	1.33	0.86	3.46	0.58	0.55	0.50
CaO %	52.05	54.33	54.93	54.88	44.28	54.16	44.23	55.21	38.26	51.77	52.87	47.77	49.74	54.07	53.45
Na_2O %	0.02	0.01	0.00	0.00	0.05	0.00	0.06	0.00	0.81	0.10	0.04	0.08	0.03	0.03	0.04
K_2O %	0.11	0.06	0.02	0.00	0.21	0.05	0.19	0.02	0.46	0.12	0.18	0.30	0.25	0.06	0.11
TiO_2%	0.03	0.02	0.00	0.00	0.04	0.02	0.05	0.00	0.25	0.08	0.04	0.09	0.06	0.00	0.03
P_2O_5%	0.02	0.00	0.00	0.02	0.03	0.01	0.00	0.00	0.04	0.02	0.01	0.00	0.02	0.00	0.06
MnO %	0.09	0.06	0.03	0.02	0.06	0.03	0.04	0.00	0.07	0.04	0.07	0.09	0.01	0.00	0.04
Cr_2O_3%	0.027	0.011	0.002	0.000	0.045	0.011	0.169	0.003	0.046	0.011	0.003	0.013	0.007	0.000	0.004
LOI %	41.5	43.5	44.0	44.2	36.6	43.9	38.4	43.7	31.8	41.8	42.8	41.8	40.5	44.2	43.4
TOT/C %	11.62	11.94	12.02	12.06	9.81	11.97	9.85	12.00	8.10	11.36	11.86	11.30	10.93	11.97	11.99
TOT/S %	0.04	0.03	0.04	0.00	0.02	0.03	0.00	0.00	0.10	0.02	0.04	0.04	0.02	0.05	0.05
SUM %	99.91	99.92	99.92	99.94	99.85	99.87	99.84	99.94	99.87	99.91	99.91	99.77	99.92	99.92	99.92
Ba	11	4	4	5	11	7	6	6	42	9	4	16	5	2	9
Ni	47	<20	26	<20	88	28	325	<20	110	22	<20	37	<20	<20	<20
Be	<1	1	2	<1	<1	<1	<1	<1	<1	1	<1	1	<1	<1	<1
Co	4.8	1.7	0.9	0.6	4.0	0.5	16.1	0.5	9.3	1.8	1.4	4.6	1.0	0.4	2.2

Table 4. *Cont.*

Sample No. % and ppm	BS1-1	BS1-2	BS2-3	BS2-6	BS3-1	BS3-3	BS4-1	BS4-7	BS5-1	BS5-3	BS6-1	BS6-3	GA-4	GA-10	GA-20
Cs	0.1	<0.1	<0.1	<0.1	0.2	<0.1	<0.1	<0.1	0.1	<0.1	0.1	0.2	0.4	<0.1	0.1
Ga	0.5	<0.5	<0.5	<0.5	<0.5	<0.5	<0.5	<0.5	2.3	<0.5	<0.5	<0.5	<0.5	<0.5	<0.5
Hf	0.2	0.1	<0.1	<0.1	0.2	<0.1	0.2	<0.1	0.6	0.2	<0.1	0.2	0.2	0.1	0.1
Nb	0.9	0.5	0.2	0.1	1.4	0.5	0.6	0.2	4.6	1.8	1.0	2.0	1.4	0.2	0.6
Rb	2.3	1.4	0.7	0.3	3.8	1.3	1.0	0.4	5.8	2.6	2.5	4.1	5.7	0.7	2.0
Sn	<1	<1	<1	<1	<1	<1	<1	<1	<1	<1	<1	<1	<1	<1	<1
Sr	496.4	520.5	520.7	397.6	890.6	858.9	417.3	408.7	332.8	426.2	572.5	1391.7	450.2	480.8	502.0
Ta	<0.1	<0.1	<0.1	<0.1	<0.1	<0.1	<0.1	<0.1	0.2	0.1	<0.1	<0.1	<0.1	<0.1	<0.1
Th	0.3	0.2	<0.2	<0.2	0.4	0.3	<0.2	<0.2	0.7	0.3	<0.2	0.4	0.6	<0.2	<0.2
U	2.6	3.4	3.0	2.1	0.9	2.5	0.7	1.7	2.2	1.4	0.7	1.9	2.5	1.6	1.1
V	27	16	15	<8	23	29	37	13	57	14	13	21	17	9	12
W	4.6	3.6	2.3	2.9	3.6	1.0	1.0	0.8	3.0	1.1	1.4	0.8	0.7	<0.5	0.7
Zr	8.1	3.6	2.2	1.6	9.4	4.6	5.3	2.2	25.0	9.0	5.5	10.3	10.1	4.4	5.7
Y	4.1	5.3	3.6	1.4	3.1	2.5	2.0	1.1	6.8	3.3	1.3	2.4	2.7	0.7	5.1
La	4.0	5.0	1.5	0.8	3.2	1.7	1.4	0.6	7.2	3.5	1.8	2.5	2.8	0.7	3.5
Ce	6.2	4.7	2.3	0.8	5.2	3.2	2.4	0.8	13.5	7.2	3.4	4.5	5.3	1.3	5.1
Pr	0.77	0.98	0.36	0.10	0.67	0.35	0.28	0.12	1.54	0.78	0.35	0.49	0.58	0.13	0.58
Nd	3.1	3.8	1.4	0.6	2.6	1.5	1.2	0.4	6.2	3.0	1.4	2.0	2.3	0.5	2.4
Sm	0.71	0.75	0.22	0.07	0.53	0.35	0.23	<0.05	1.40	0.67	0.28	0.39	0.43	0.14	0.44
Eu	0.19	0.20	0.08	0.03	0.12	0.08	0.08	0.03	0.38	0.20	0.08	0.11	0.11	0.03	0.18
Gd	0.66	0.81	0.29	0.15	0.58	0.43	0.31	0.11	1.37	0.66	0.28	0.38	0.49	0.11	0.60
Tb	0.13	0.12	0.06	0.02	0.08	0.05	0.05	0.01	0.20	0.09	0.04	0.05	0.07	0.01	0.08
Dy	0.54	0.65	0.30	0.15	0.46	0.35	0.36	0.10	1.19	0.48	0.21	0.40	0.42	0.10	0.61
Ho	0.14	0.13	0.08	<0.02	0.11	0.06	0.08	0.03	0.26	0.11	0.05	0.07	0.07	0.02	0.12
Er	0.33	0.33	0.19	0.10	0.30	0.15	0.24	0.08	0.69	0.29	0.12	0.22	0.18	0.06	0.38
Tm	0.07	0.05	0.03	<0.01	0.04	0.03	0.03	<0.01	0.10	0.04	0.02	0.03	0.03	<0.01	0.04
Yb	0.28	0.25	0.16	0.06	0.26	0.14	0.21	0.06	0.58	0.26	0.13	0.17	0.20	<0.05	0.25
Lu	0.06	0.05	0.03	<0.01	0.04	0.02	0.03	<0.01	0.10	0.04	0.01	0.02	0.03	<0.01	0.04
Sc	1	<1	<1	<1	2	<1	4	<1	8	2	1	2	1	<1	<1

Based on their $MgCO_3$ and $CaCO_3$ contents, the carbonate samples were classified as limestone or dolomitic limestone (Table 5). Among the Besni Formation samples, two were identified as dolomitic limestone, including two sandy dolomitic limestone samples (BS4-1 and BS5-1), whereas the remaining ten samples were classified as limestone, one of which was identified as sandy limestone (BS3-1). All samples from the Garzan Formation were classified as limestone, except for sample GA-4, which was identified as sandy limestone (Table 5).

Table 5. $MgCO_3$% and $CaCO_3$% contents of the Besni and Garzan formations.

Sample No.	$MgCO_3$%	$CaCO_3$%	Explanations
BS1-1	0.85	99.15	Limestone
BS1-2	0.69	99.31	Limestone
BS2-3	0.59	99.41	Limestone
BS2-6	0.49	99.51	Limestone
BS3-1	5.22	94.78	Limestone (Sandy)
BS3-3	1.20	98.80	Limestone

Table 5. *Cont.*

Sample No.	$MgCO_3$%	$CaCO_3$%	Explanations
BS4-7	0.86	99.14	Limestone
BS5-3	2.92	97.08	Limestone
BS6-1	1.87	98.13	Limestone
BS6-3	7.83	92.17	Limestone
BS4-1 (dol lms)	13.66	86.34	Dolomitic Limestone (Sandy)
BS5-1 (dol lms)	10.11	89.89	Dolomitic Limestone (Sandy)
GA-4	1.35	98.65	Limestone (Sandy)
GA-10	1.18	98.82	Limestone
GA-20	1.08	98.92	Limestone

4.4. Trace-Rare Earth Element Geochemistry

The trace element concentrations of samples from both formations are presented in Table 6. Overall, the Besni and Garzan formations exhibit comparable trace and minor element compositions (Table 6). To evaluate the Ce and Eu anomalies of the samples, the following equations were used (Equation (1) [43,44]; Equation (2) [44]:

$$Ce/Ce^* = [Pr \times (Pr/Nd)Ce]SN \quad (1)$$

$$Eu/Eu^* = EuN/[Sm2N^*TbN]1/3 \quad (2)$$

Table 6. Ba, Rb, Si, Al, Fe, Na, ΣREE, ΣLREE, ΣHREE, Ce/Ce*, Eu/Eu* and Y/Ho contents of carbonate rocks in the Besni and Garzan formations.

Sample No.	Ba (ppm)	Rb (ppm)	Si (ppm)	Al (ppm)	Fe (ppm)	Na (ppm)	Σ REE	Σ LREE	Σ HREE	Ce/Ce*	Eu/Eu*	Y/Ho
BS1-1	11	2.3	21,269	1217	4476	74	17.18	15.63	1.55	1.00	1.24	29.29
BS1-2	4	1.4	4861	741	2238	37	17.82	16.24	1.58	0.58	1.29	40.77
BS2-3	4	0.7	1683	212	1399	0	7.00	6.15	0.85	0.77	1.47	45.00
BS2-6	5	0.3	2057	53	629	0	2.88	2.55	0.33	1.49	1.71	0.00
BS3-1	11	3.8	70,117	1932	5386	185	14.19	12.90	1.29	0.93	1.12	28.18
BS3-3	7	1.3	3132	423	2308	0	8.41	7.61	0.80	1.21	1.15	41.67
BS4-1	6	1.0	37,255	2540	12,100	223	6.90	5.90	1.00	1.14	1.52	25.00
BS4-7	6	0.4	1776	185	769	0	2.34	2.06	0.28	0.69	0.00	36.67
BS5-1	42	5.8	87,553	9289	15,598	3005	34.71	31.59	3.12	1.09	1.36	26.15
BS5-3	9	2.6	14,351	2196	4896	371	17.32	16.01	1.31	1.10	1.53	30.00
BS6-1	4	2.5	9770	1270	2868	148	8.17	7.59	0.58	1.20	1.44	26.00
BS6-3	16	4.1	19,820	2567	6645	297	11.33	10.37	0.96	1.16	1.47	34.29
GA-4	5	5.7	34,124	2461	3427	111	13.01	12.01	1.00	1.12	1.23	38.57
GA-10	2	0.7	3786	238	350	111	3.10	2.91	0.19	1.19	1.36	35.00
GA-20	9	2.0	7245	715	3567	148	14.32	12.80	1.52	1.13	1.90	42.50

The carbonate rock samples from the Besni Formation generally exhibited positive Ce anomalies, with Ce/Ce values ranging from 0.58 to 1.49 (mean = 1.03). Only four samples displayed negative Ce anomalies, with Ce/Ce values between 0.58 and 0.93 (Table 6). Eu anomaly values (Eu/Eu*) ranged from 0.00 to 1.71 (mean = 1.28) and were predominantly positive. The carbonate samples showed slight enrichment in light rare earth elements (ΣLREE) and relative depletion in heavy rare earth elements (ΣHREE) (Figure 9).

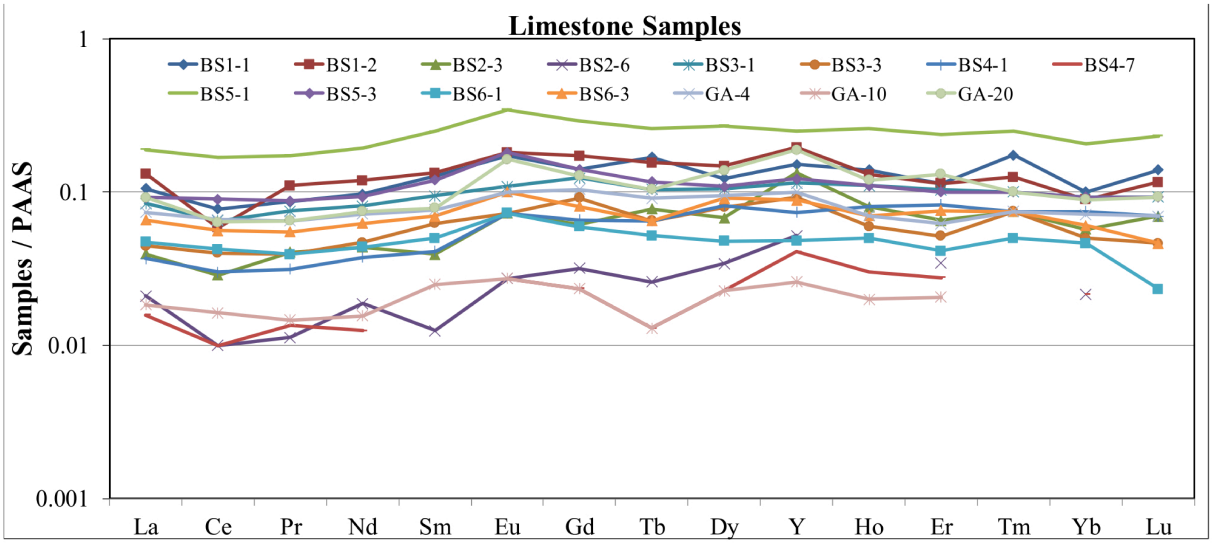

Figure 9. Diagram rare earth elements (REE + Y) showing Normalized [45] Post-Archean Australian Shale (PAAS) values of carbonate rocks in the Besni and Garzan formations.

The carbonate rock samples from the Garzan Formation exhibited positive Ce anomalies, with Ce/Ce values ranging from 1.12 to 1.19 (mean = 1.15). Eu anomaly values (Eu/Eu) ranged from 1.23 to 1.90 (mean = 1.50), indicating consistently positive Eu anomalies (Table 6). The carbonate samples showed slight enrichment in light rare earth elements (ΣLREE) and relative depletion in heavy rare earth elements (ΣHREE) (Figure 9). The carbonate rocks of the Besni Formation exhibited Y/Ho ratios of 25.00–45.00 (mean = 33.00), except for one sample with a ratio of 0. In the Garzan Formation, Y/Ho ratios varied between 35.00 and 42.50 (mean = 38.39) (Table 6).

4.5. $\delta^{18}O$ and $\delta^{13}C$ Isotopes and Temperature

The carbonate rocks of the Besni Formation exhibited $\delta^{18}O$ values ranging from −2.82‰ to −6.69‰ (VPDB) and $\delta^{13}C$ values from −0.83‰ to +3.23‰ (VPDB) (Table 7). The carbonate rocks of the Garzan Formation yielded $\delta^{18}O$ values between −3.65‰ and −5.96‰ (VPDB) and $\delta^{13}C$ values ranging from +0.89‰ to +3.39‰ (VPDB) (Table 7).

Table 7. To, Z, $\delta^{18}O$ and $\delta^{13}C$ (PDB) values of carbonate rocks in the Besni and Garzan formations.

Sample No.	$\delta^{13}C$ (‰) vs. VPDB	$\delta^{18}O$ (‰) vs. VPDB	T° Temperature	Z Value
BS1-1	0.28	−5.81	45	125
BS1-2	0.69	−5.69	44	126
BS2-3	0.60	−5.67	44	126
BS2-6	0.07	−5.48	43	125
BS3-1	1.59	−4.63	38	128
BS3-3	2.66	−4.69	39	130
BS3-5	1.99	−5.62	44	129
BS3-7	2.07	−5.36	43	129
BS3-9	1.43	−5.90	46	127
BS3-11	1.31	−6.29	48	127
BS4-1	2.43	−3.75	34	130

Table 7. *Cont.*

Sample No.	$\delta^{13}C$ (‰) vs. VPDB	$\delta^{18}O$ (‰) vs. VPDB	T° Temperature	Z Value
BS4-7	3.23	−4.77	39	132
BS4-11	2.76	−4.55	38	131
BS5-1	1.84	−3.92	35	129
BS5-3	2.38	−3.75	34	130
BS6-1	0.95	−4.55	38	127
BS6-3	-0.83	−4.51	38	123
BS6-4	-0.78	−6.69	50	122
GA4	1.82	−5.96	46	122
GA6	2.67	−3.65	33	128
GA10	3.39	−4.51	38	131
GA18	1.44	−5.22	42	132
GA20	0.89	−4.41	37	128

Paleotemperatures of the carbonate rocks were calculated using the oxygen isotope paleotemperature equation of Epstein and Mayeda [46], as modified by Craig [47] and Hayes and Grossman [48]:

$$T(°C) = 15.7 - 4.36(\delta^{18}O_{calcite-water}) + 0.12(\delta^{18}O_{calcite-water})^2$$

Calculated formation temperatures range from 34 to 50 °C (mean = 41 °C) for the Besni Formation and from 33 to 46 °C (mean = 39 °C) for the Garzan Formation (Table 7).

For Jurassic and younger limestones, assuming that the samples have not undergone significant recrystallization, the most reliable discrimination between marine and freshwater carbonates can be achieved using the Z parameter proposed by Keith and Weber [49]:

$$Z = 2.048(\delta^{13}C + 50) + 0.498(\delta^{18}O + 50)$$

where both $\delta^{13}C$ and $\delta^{18}O$ values are expressed relative to the VPDB standard [49,50]. Limestone samples with Z values greater than 120 are interpreted as having precipitated in marine environments, whereas those with Z values below 120 are considered to represent freshwater deposition [50,51]. For older geological successions, however, marine and freshwater carbonates may be more reliably distinguished using carbon isotope compositions alone [50].

The calculated Z values of the carbonate rock samples from the Besni and Garzan formations range from 122 to 132 (Table 7), indicating a marine origin for all analyzed samples. The cross-plot of the $\delta^{18}O$ versus $\delta^{13}C$ values for the investigated carbonate samples is shown in Figure 10.

These results suggest that the carbonate rocks have experienced only limited burial diagenesis, and that their primary isotopic compositions may have been largely preserved. The calculated temperatures (34–50 °C) are interpreted as apparent temperatures. Because they are higher than expected for Maastrichtian tropical seawater, they likely include a diagenetic (burial) overprint and the effect of cements, and are not used to infer climatic change [52,53].

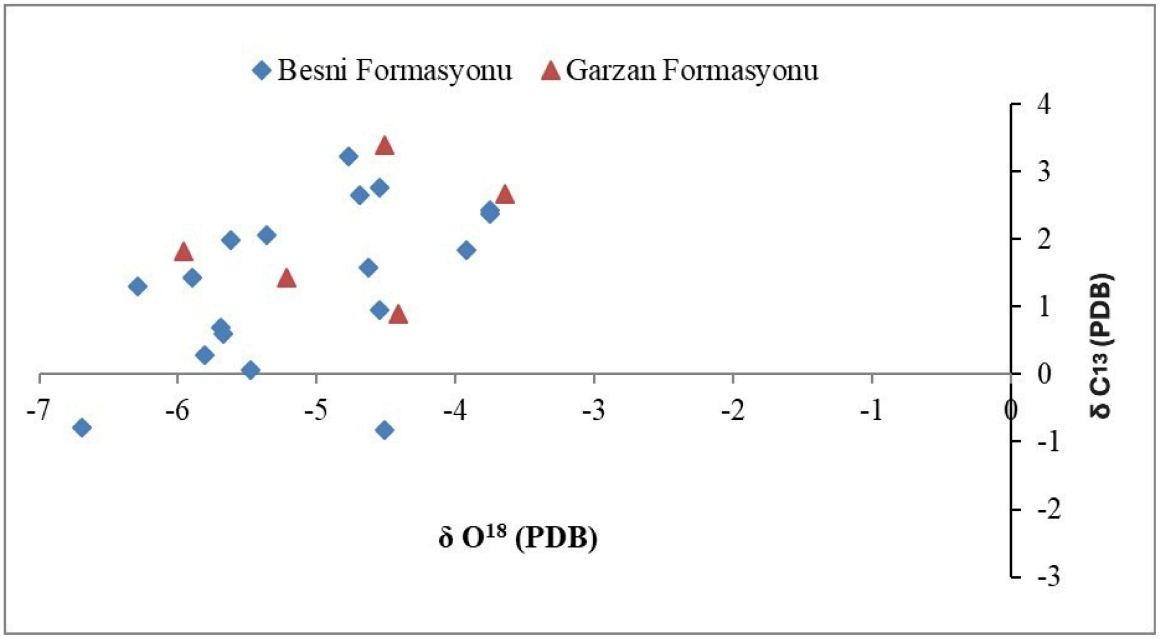

Figure 10. Comparison of $\delta^{18}O$ and $\delta^{13}C$ (PDB) isotope values of carbonate rocks in the Besni and Garzan formations.

4.6. Paleontological Results

Benthic foraminifera constitute an important component of tropical shallow-water carbonate systems and have been widely used in stratigraphic evolutionary models. Although their tests exhibit complex morphological architectures, these structures provide the fundamental basis for taxonomic classification [54,55]. Owing to their wide geographic distribution and relatively rapid evolutionary rates throughout geological time, benthic foraminifera represent excellent index fossils and provide robust data for stratigraphic studies based on larger benthic foraminifera (LBF) [55]. In addition, foraminifera are widely used to investigate past extinction events by providing insights into global (eustatic) sea-level fluctuations and climate change. Because they inhabit almost all marine environments and occupy a wide range of shelf settings, they provide unique information on paleoenvironmental conditions and stratigraphic evolution. Representative examples include Fusulinids and Schwagerinids from the Upper Paleozoic, Orbitoids from the Middle–Upper Cretaceous, Nummulitids from the Paleogene, and Lepidocyclinids and Miogypsinids from the Oligocene and Neogene.

4.6.1. Besni Formation

The Besni Formation is exposed around Taşyazı, Besni, Palanlı, Dumlu, and Alidam in Adıyaman Province (Figure 1). It is composed mainly of light beige to cream-coloured bioclastic limestones containing abundant larger benthic foraminifera and other skeletal fragments. Six measured sections (BS1–BS6) were established across these outcrops.

The measured sections yielded a diverse assemblage of benthic foraminifera, represented by *Loftusia kahtaensis* Meriç, *Orbitoides medius* (d'Archiac), *Omphalocyclus macroporus* (Lamarck), *Lenticulina rotulata* Lamarck, *Sirtina ornata* Rahaghi, *Fissoelphidium operculiferum* Smout; *Elazigina siderea* Consorti and Rashidi, *Siderolites calcitropoides* Lamarck, *Stomatorbina* sp., *Goupilloidina* sp., *Kolchidina* sp., *Valvulineria* sp., *Orbitoides* sp., and *Hadonnia* sp. (Figures 11A–O and 12A–F).

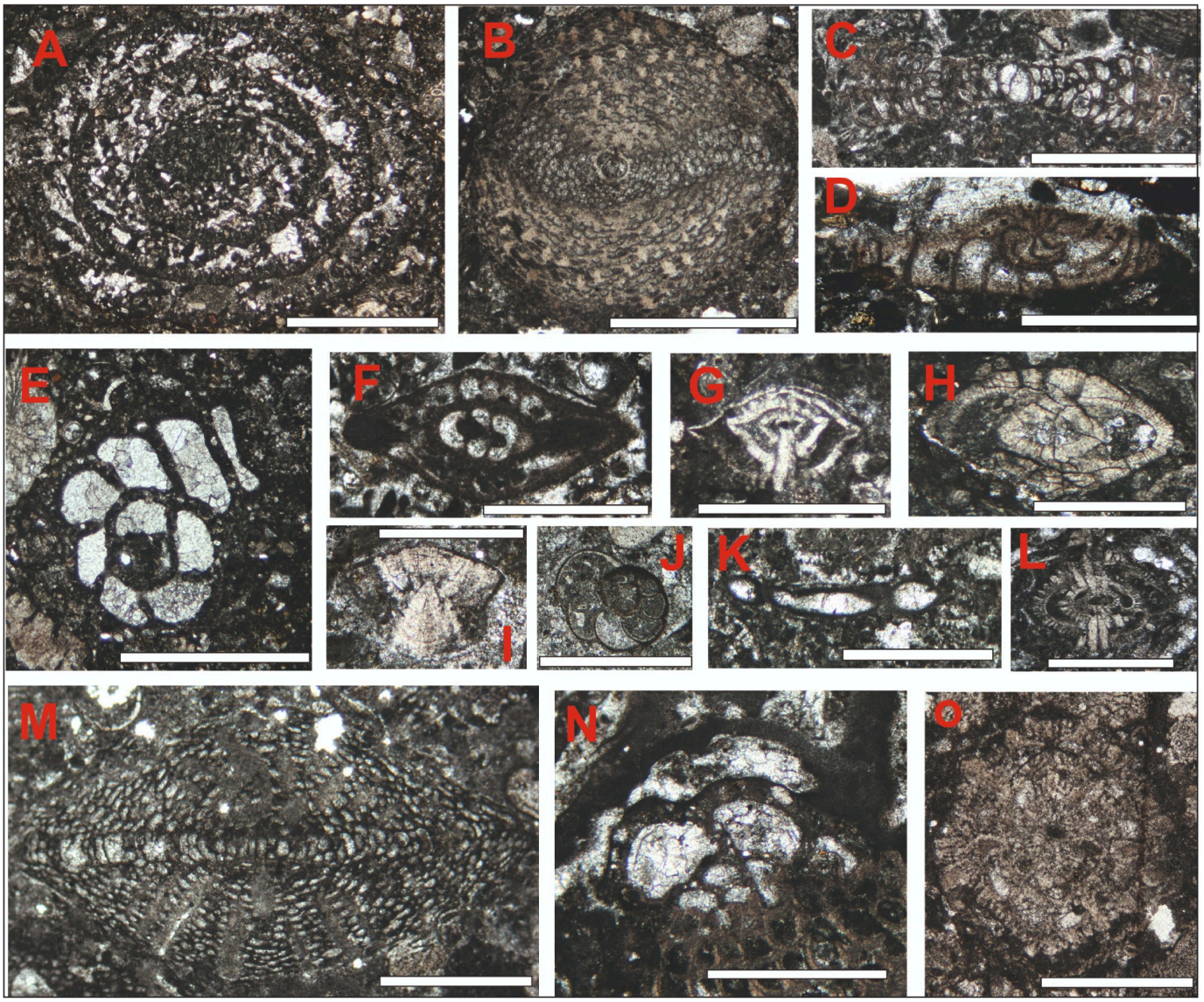

Figure 11. Benthic foraminifera assemblage of the Besni Formation: (**A**) *Loftusia kahtaensis*; (**B**) *Orbitoides medius*; (**C**) *Omphalocyclus macroporus*; (**D**) *Goupilloidina* sp.; (**E**) *Kolchidina* sp.; (**F**) *Lenticulina rotulata*; (**G**) *Sirtina ornata*; (**H**) *Fissoelphidium operculiferum*; (**I**) *Elazigina siderea*; (**J**) *Valvulineria* sp.; (**K**) *Stomatorbina* sp.; (**L**,**O**) *Siderolites calcitropoides*; (**M**) *Orbitoides* sp.; (**N**) *Hadonnia* sp. Scale bar: 1000 μm.

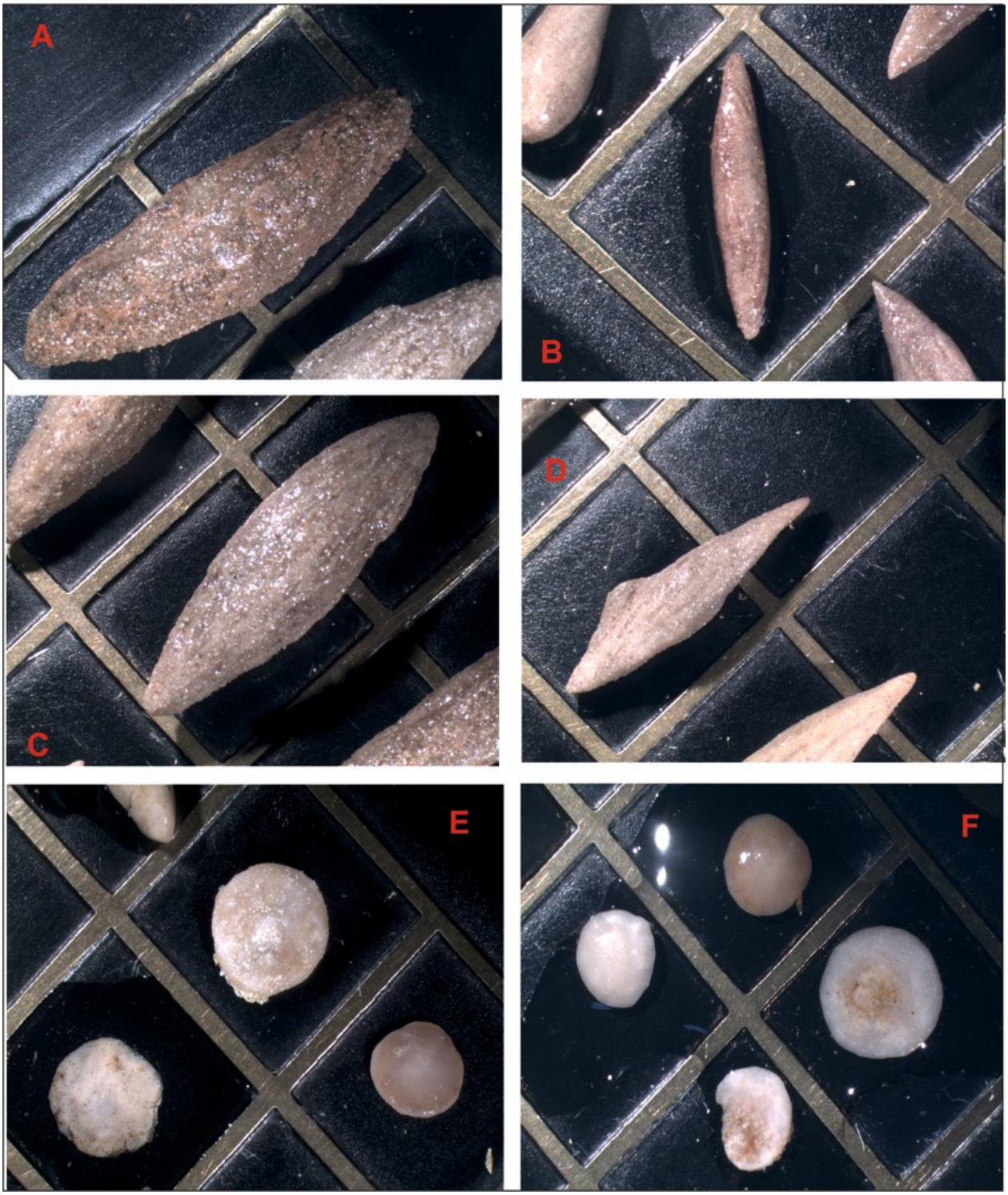

Figure 12. Larger benthic foraminifera specimens from the Besni Formation: (**A**–**D**) *Loftusia* sp.; (**E**,**F**) orbitoid forms.

4.6.2. Garzan Formation

The Garzan measured stratigraphic section is located approximately 15 km west of the Gercüş District in southeastern Batman Province, within the core of the Gercüş Anticline. Although the basal contact of the Garzan Formation is not exposed in the study area, drilling data indicate that the underlying unit consists of the Kıradağ Formation, which is composed of shale, sandstone, and marl. The measured section begins with well-bedded to massive limestones at the base. Upsection, these limestones gradually pass into nodular limestones

in the middle part of the section. Toward the upper part, increasing clay content results in a gradual transition into the Germav Formation, represented by calcareous siltstone, marl, and shale lithologies. The total thickness of the measured section is approximately 126 m.

Throughout the measured section, porcelaneous, microgranular, and agglutinated benthic foraminiferal taxa, including *Orbitoides megaloformis* Papp and Küpper, *Orbitoides medius* (d'Archiac), *Siphopfenderina geyikensis* (Solak), *Fleuryana adriatica* (De Castro), *Sirtina orbitoidiformis* Brönnimann and Wirtz, *Trochospira avnimelechi* Hamaoui, *Cuneolina ketini* İnan, *Dicyclina schlumbergeri* Munier-Chalmas, *Vandenbroekia munieri* Marie, *Nezzazatinella picardi* (Henson), *Moncharmontia apenninica* (De Castro), *Dictyoconella complanata* Henson, *Antalyna korayi* Farinacci and Köylüoğlu, *Pseudomphalocyclus blumenthali* Meriç, and *Omphalocyclus* sp. occur from the basal levels of the unit. However, their relative abundance varies throughout different stratigraphic intervals. The same levels also contain abundant dasycladalean algae associated with these foraminiferal taxa (Figure 13A–O).

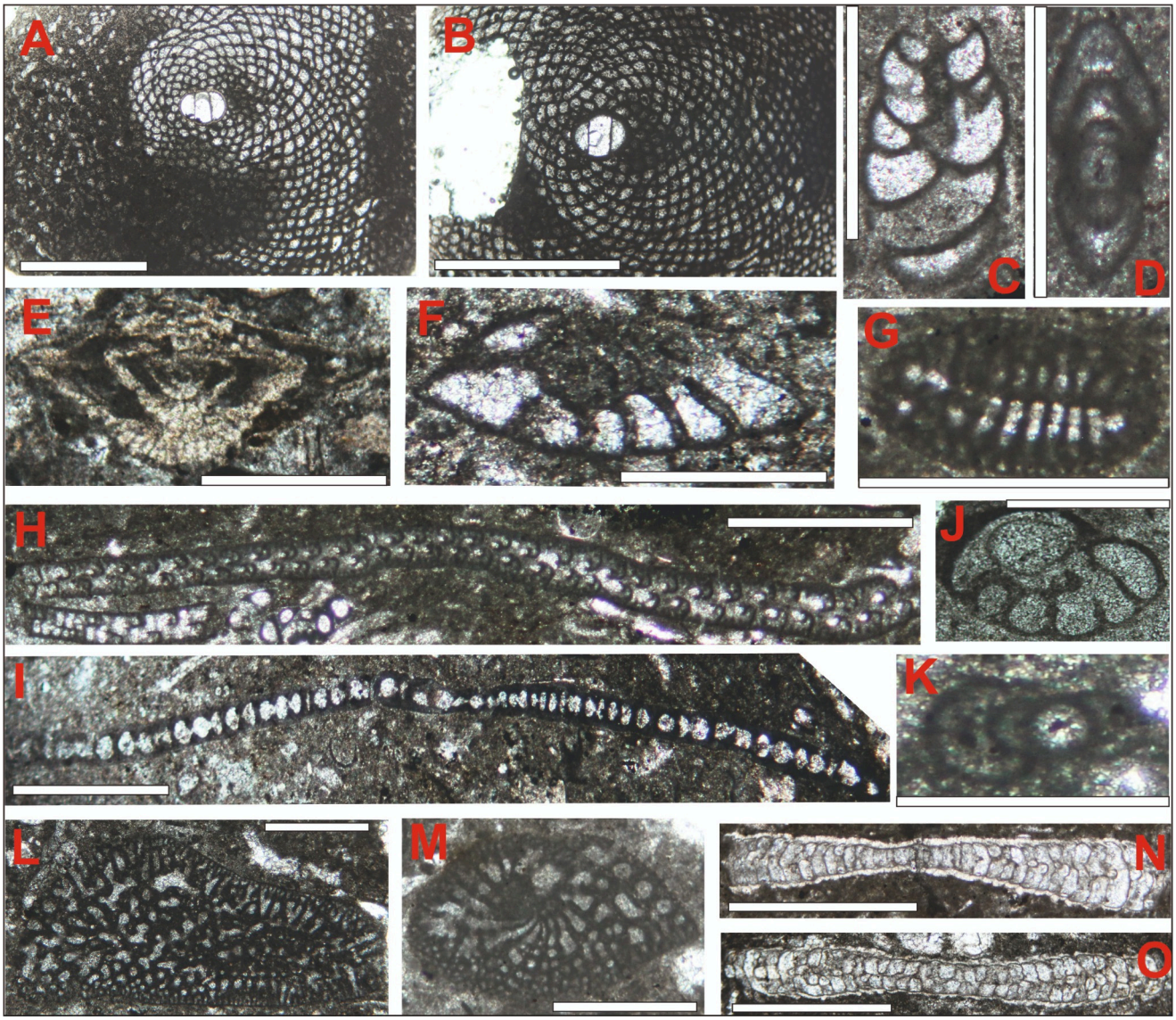

Figure 13. Benthic foraminifera assemblage of the Garzan Formation: (**A**) *Orbitoides megaloformis*; (**B**) *Orbitoides medius*; (**C**) *Siphopfenderina geyikensis*; (**D**) *Fleuryana adriatica*; (**E**) *Sirtina orbitoidiformis*; (**F**) *Trochospira avnimelechi*; (**G**) *Cuneolina ketini*; (**H**) *Dicyclina schlumbergeri*; (**I**) *Vandenbroekia munieri*; (**J**) *Nezzazatinella picardi*; (**K**) *Moncharmontia apenninica*; (**L**) *Dictyoconella complanata*; (**M**) *Antalyna korayi*; (**N**) *Pseudomphalocyclus blumenthali*; (**O**) *Omphalocyclus* sp. Scale bar: 1000 µm.

5. Discussion

5.1. Petrographic Analyses

In the study area, the limestones of the Besni Formation either directly overlie the turbiditic deposits of the Kastel Formation or the coarse-grained clastic facies of the Terbüzek Formation (Figure 1). Rudist bivalves, benthic foraminifera, gastropods, and algal fragments are commonly observed throughout the formation. Based on their components and textures, the carbonate rocks are grouped into the following facies: (1) bioclastic packstone and grainstone with abundant larger benthic foraminifera, rudist and coral fragments and intraclasts (Besni Formation), indicating winnowing and relatively high energy; (2) sandy and sandy dolomitic limestones containing detrital quartz and other non-carbonate grains, indicating siliciclastic input; (3) bioclastic packstone with porcelaneous, microgranular and agglutinated foraminifera and dasycladalean algae in a micritic matrix (Garzan Formation), indicating a relatively more protected, lower-energy setting. These facies and their vertical succession are interpreted as recording relatively high-energy versus relatively protected shallow-marine conditions (Tables 2 and 3). The larger benthic foraminiferal assemblages identified in the Besni and Garzan formations are consistent with warm, shallow-marine carbonate-platform environments. However, their distribution is influenced by several environmental factors, including temperature, water depth, light availability, salinity, and hydrodynamic energy. Therefore, these assemblages provide qualitative paleoenvironmental constraints rather than precise quantitative paleotemperature estimates.

The Besni and Garzan formations represent different sectors of the same Late Maastrichtian Arabian carbonate platform.

This interpretation is consistent with the broader Maastrichtian carbonate-platform system developed along the northern margin of the Arabian Plate. Comparable shallow-marine carbonate successions, including the Tarbur Formation of the Zagros Basin, the Aqra Formation of northern Iraq, the Hartha Formation of Iraq, and the Simsima Formation of the southeastern Arabian Peninsula, contain abundant larger benthic foraminifera, rudists, algae, and skeletal limestones [55–58]. The occurrence of *Loftusia*, *Orbitoides*, *Omphalocyclus*, and *Siderolites* in the Besni and Garzan formations is consistent with their regional affinity to Maastrichtian carbonate platforms of the eastern Neo-Tethys [55,59]. Despite differences in thickness, facies architecture, and tectonic setting, these successions record the development of shallow-marine carbonate systems along the northern margin of the Arabian Plate. The petrographic, paleontological, and geochemical differences observed between the Besni and Garzan formations are therefore interpreted as local variations in hydrodynamic energy, carbonate production, accommodation space, and siliciclastic input within a broader regional carbonate-platform system [57,58,60].

5.2. Analyses Major-Trace Elements

The SiO_2 contents of the samples from the Besni Formation range from 0.36 to 18.73 wt.% (Table 4). The high SiO_2 concentrations in carbonate rocks suggest the contribution of silica-rich mineral phases associated with the input of detrital material during limestone deposition. Limestone samples with MgO contents exceeding 3 wt.% indicate the presence of dolomitization. In the mol% $MgCO_3$–Sr (ppm) diagram, the relationship between Sr and $MgCO_3$ contents in the carbonate samples from the Besni and Garzan formations shows that Sr concentrations increase with increasing $MgCO_3$ content (Figure 14A). In the Fe–Sr (ppm) diagram, Sr concentrations increase with increasing Fe contents in limestones, whereas they decrease with increasing Fe contents in dolomitic limestones (Figure 14B). In the CaO–Fe (ppm) diagram, Fe concentrations decrease with increasing $CaCO_3$ contents in limestones (Figure 14C).

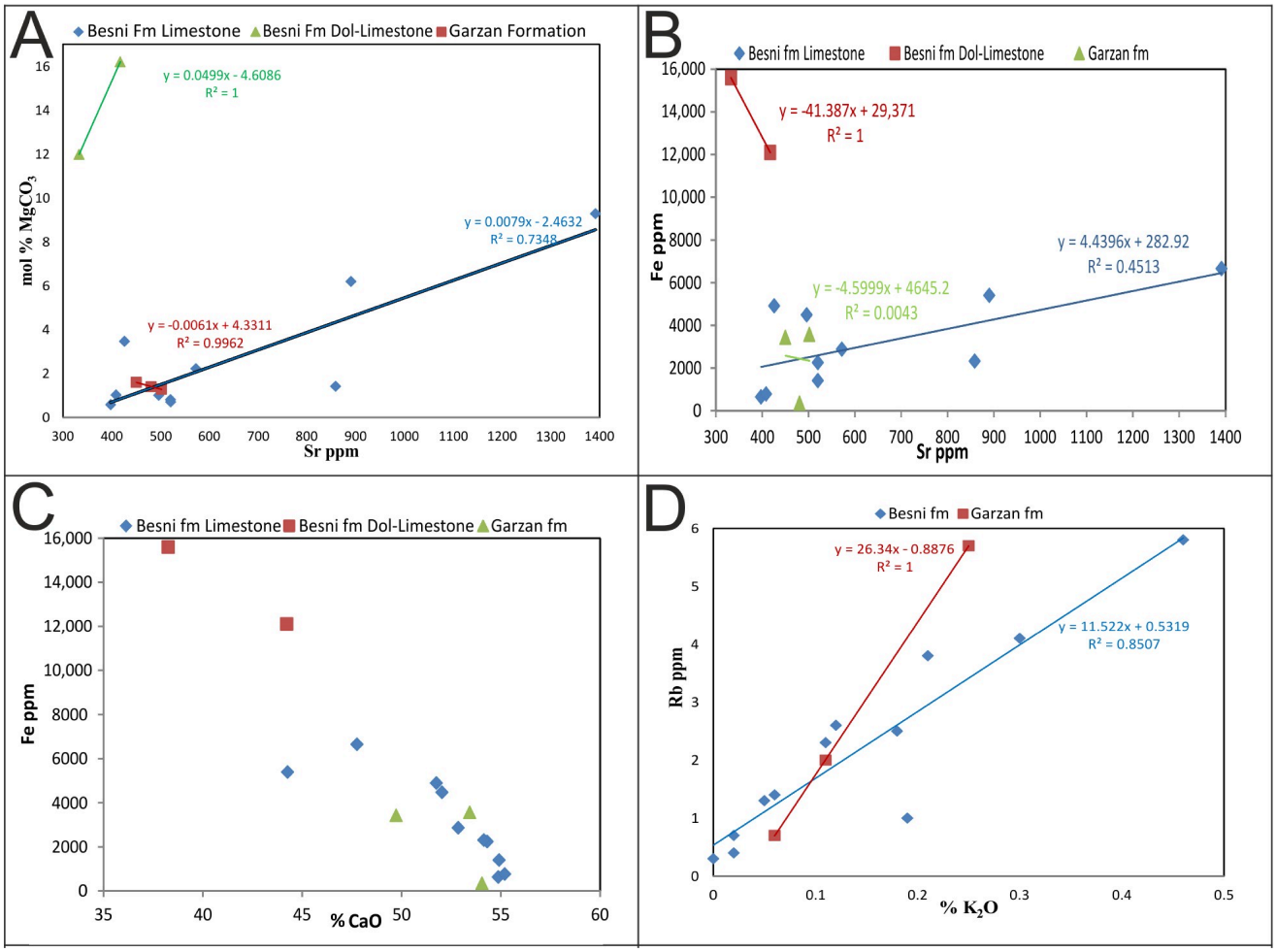

Figure 14. (**A**) $MgCO_3$% versus Sr (ppm) plot. (**B**) Fe versus Sr (ppm) plot. (**C**) CaO% versus Fe (ppm) plot. (**D**) K_2O%–Rb (ppm) plot.

Marine calcites generally contain approximately 1000 ppm Sr, whereas dolomites contain about half of this amount; in contrast, aragonite may contain up to approximately 10,000 ppm Sr [61]. Brand and Veizer [62] demonstrated that the recrystallization of aragonite results in Sr depletion. The Sr concentrations of carbonate rocks from the Besni Formation range from 333 to 1392 ppm (mean: 603 ppm), whereas those of the Garzan Formation range from 450 to 502 ppm (mean: 478 ppm) (Tables 4 and 6). These data suggest that the carbonate rocks of both formations were originally deposited in marine environments. Rubidium (Rb) concentrations vary depending on clay mineralogy [61]. Rb is present in highest concentrations in illite, moderate concentrations in kaolinite, and in the lowest concentrations in montmorillonite [63,64]. Degens et al. [65] and Rao [63] reported that variations in Rb concentrations from marine to freshwater environments are largely controlled by the illite/kaolinite ratio and the substitution of Rb for K in illite. The replacement of K by Rb in illite results in a positive correlation between Rb contents and K_2O concentrations. This positive correlation indicates that the clay minerals within the carbonate rocks are of marine origin [63]. A similar positive correlation between Rb contents and K_2O concentrations was observed in our samples (Figure 14D). Therefore, this relationship supports a marine depositional origin for the carbonate rocks of both formations. Friedman [66] and Rao [63] reported that recent marine limestones generally contain low Ba concentrations (<60 ppm), whereas freshwater limestones exhibit higher Ba concentrations (>60 ppm). In the present study, Ba concentrations of the carbonate rocks from the Besni Formation ranged from 4 to 42 ppm (mean: 10 ppm), while those from the

Garzan Formation ranged from 2 to 9 ppm (mean: 5 ppm) (Table 4). Since the Ba contents of carbonate rocks from both the Besni and Garzan formations were below 60 ppm, these results further support a marine depositional environment for the studied carbonates.

5.3. Rare Earth Elemental Analyses

Mirza et al. [67] reported that PAAS-normalized REE concentrations in the Avroman limestones are relatively low, with total REE (ΣREE) values ranging from 5.98 to 17.45 (mean: 11.23). Schieber [68] suggested that REE enrichment during the potential syn-sedimentary precipitation of carbonate rocks from seawater is generally very limited. Mirza et al. [67] further indicated that any REE enrichment observed in carbonate rocks is likely associated with diagenetic alteration. Compared with LREEs (La, Ce, Pr, Nd, Sm, Eu, and Gd), HREEs (Tb, Dy, Ho, Er, Tm, Yb, and Lu) in the Avroman limestones show a slight enrichment trend. This enrichment is associated with negative Ce anomalies, slightly positive La anomalies, and positive Eu and Y anomalies. The occurrence of negative Ce, positive La, Eu, and Y anomalies, together with HREE enrichment, indicates that the Avroman limestones were deposited under oxic conditions. Low REE concentrations and negative Ce anomalies suggest that limestones and dolomites were deposited in oxygenated open-marine environments away from terrestrial source materials [69]. Tostevin et al. [70] reported that shale-normalized REE patterns of modern seawater are characterized by negative Ce anomalies [71], with Ce/Ce values ranging from 0.4 to 0.7 [72]. As emphasized by Shields and Stille [73], Ce anomalies are sensitive indicators of redox conditions during the deposition of marine sediments. However, Ce anomalies may be affected by late diagenetic processes [74].

Ce anomalies are widely used to evaluate the redox conditions of depositional environments. Negative Ce anomalies may indicate oxidizing conditions during dolomitization or the removal of Ce from dolomitizing fluids within an oxidizing environment prior to dolomitization [75]. Elderfield and Greaves [72] and Piepgras and Jacobsen [76] reported that Ce/Ce values in ocean waters range from <0.1 to 0.4, whereas the average Ce/Ce value in shales is approximately 1 [77]. According to Madhavaraju and Lee [78], Ce/Ce* values below 1 in REE patterns represent negative Ce anomalies. Negative Ce anomalies indicate that the contribution of the primary sediment source was influenced by inputs derived from the water column [67,79,80]. Tostevin et al. [70] suggested that negative Ce anomalies, which are commonly observed in modern oxygenated waters and preserved in carbonate sediments and rocks, provide strong evidence for deposition under oxic conditions. In pristine marine systems, Ce anomalies greater than 1 are typically utilized to infer the presence of anoxic conditions [81]. However, as emphasized by modern literature, such positive shifts do not exclusively dictate bottom-water anoxia and can frequently reflect detrital overprinting, diagenetic alteration, or fluctuating paleo-redox conditions [78,82–84]. In general, carbonate rocks precipitated from oxygen-rich seawater exhibit negative Ce anomalies, whereas strongly positive Ce anomalies may be observed in carbonates deposited under oxygen-depleted conditions [81,85–87].

Lawrence et al. [44] reported the occurrence of both positive (Mooloolah River, Eu: 1.15) and negative Eu anomalies (Tibrogargan Creek, Eu: 0.42) in their studied samples. Positive Eu anomalies in dolomites are generally considered indicative of hydrothermal dolomitization [88,89]. The REE compositions of modern clastic sediments and marine chemical precipitates mainly reflect the composition of the upper continental crust, which is characterized by negative Eu anomalies [72,90]. PAAS-normalized positive Eu anomalies are uncommon in seawater [91]. Positive Eu anomalies may originate from hydrothermal fluids [91–95], diagenetically altered sediments [96], feldspar enrichment [77,78,82,84,97], and sediments derived from high-temperature basalt alteration along mid-ocean ridges or

back-arc spreading centers [90,91,94,98]. In particular, negative Eu anomalies may occur in dolomites when hydrothermal fluids are derived from intermediate-acidic magmatic sources [99,100].

As shown in the plots illustrating the relationships between major elements and total REE contents of the carbonate rocks from the Besni and Garzan formations, a weak negative correlation was observed between total REE and CaO (Figure 15A), whereas positive correlations were observed with SiO_2, Al_2O_3, and Fe (Figure 15B–D). In addition, carbonate rock samples from both formations exhibited REE depletion (Tables 4 and 6; Figure 9).

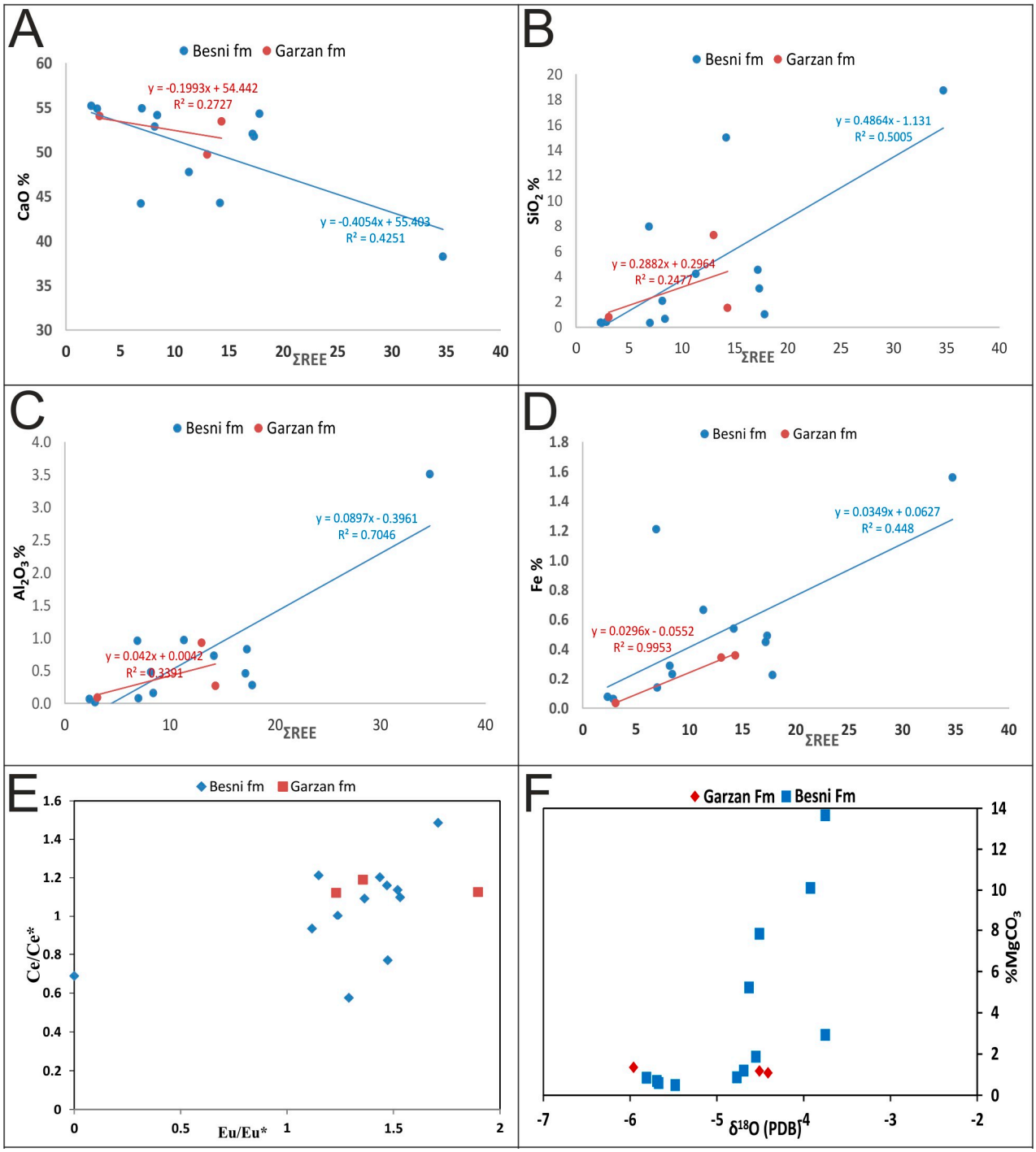

Figure 15. (**A**) CaO% versus ΣREE plot. (**B**) SiO_2% versus ΣREE plot. (**C**) Al_2O_3% versus ΣREE plot. (**D**) Fe% versus ΣREE plot. (**E**) Ce/Ce* versus Eu/Eu* plot. (**F**) ‰$\delta^{18}O$ (PDB) versus $MgCO_3$% plot.

The carbonate rocks of the Besni Formation in the study area exhibit variable Ce anomalies, with predominantly positive values (n = 8) and negative values (n = 4), together with positive Eu anomalies (mean: 1.28) (Figure 15E; Table 6). The average Ce anomaly value of the carbonate rocks from the Besni Formation is 1.03. Carbonate rocks of the Garzan Formation display positive Ce anomalies (mean: 1.15) and positive Eu anomalies (mean: 1.50) (Figure 15E; Table 6).

To the best of our knowledge, this study represents the premier geochemical investigation of its kind in the region. Although a constrained suite of major and trace element analyses was performed on samples from both formations, these preliminary data permit an initial comparison with existing regional literature. Given these data limitations, the interpretations regarding both Ce and Eu anomalies should not be viewed as definitive redox indicators, but rather as a preliminary conceptual approach that requires further validation.

Consequently, because the Ce/Ce* values of the Garzan Formation (1.12–1.19) and most Besni samples (1.00–1.21) are close to unity, and the positive correlations between ΣREE and SiO_2, Al_2O_3 and Fe (Figure 15B–D) indicate detrital contamination, a categorical redox assignment cannot be justified. Many REE concentrations are near the detection limits. These data therefore cannot support a robust redox interpretation, and the Ce anomalies are regarded as inconclusive. The low ΣREE, together with the fossil assemblages of an open, shallow-marine platform, does not point to persistent anoxic bottom waters. Positive Eu anomalies may reflect detrital feldspar, diagenesis or hydrothermal input, but our data do not discriminate between these (Table 6).

5.4. $\delta^{18}O$ and $\delta^{13}C$ Isotopes and Temperature

Typically, $\delta^{13}C$ values between 0 and +4‰ (PDB) in carbonate rocks are indicative of a marine origin [101]. Adelabu et al. [51] reported that the $\delta^{13}C$ values of the Paleocene–Eocene Ewekoro limestones (+1.9 to −1.4‰ PDB) are comparable to those of marine limestones. In general, limestones exposed to subaerial conditions at or near the surface (e.g., alterations related to meteoric diagenesis) exhibit more negative $\delta^{13}C$ values than limestones precipitated several meters below the surface [102,103]. High algal productivity and photosynthetic activity in shallow marine marginal environments result in positive $\delta^{13}C$ values [104,105], whereas the presence of organic matter may lead to more negative $\delta^{13}C$ values [104]. Positive $\delta^{13}C$ values in limestones reflect shallow marine marginal environments [51], whereas negative $\delta^{13}C$ values may be related to perturbations in oceanic productivity across the Cretaceous–Paleogene boundary, as suggested by Marshall [106], or to the isotopic enrichment of organically derived carbon during regression and erosion-related changes in the carbon cycle [51,107].

The $\delta^{18}O$ values of the Paleocene–Eocene Ewekoro limestones (−0.8 to −3.5‰ PDB) fall within the range of marine limestones and are comparable to the values reported by Veizer [51,108]. Cuna et al. [50] stated that the $\delta^{18}O$ isotopic compositions of freshwater carbonate rocks are generally depleted compared to those of marine waters. Furthermore, negative $\delta^{18}O$ values are considered indicative of meteoric water diagenesis [104]. Diagenetic processes commonly result in negative $\delta^{18}O$ values in marine carbonates because cementation and recrystallization generally occur in fluids depleted in $\delta^{18}O$ relative to seawater (e.g., meteoric waters) or under elevated temperatures during burial conditions [51,104,106]. The decrease in $\delta^{18}O$ values is associated with reduced salinity and increased temperature [109]. In general, negative $\delta^{18}O$ values observed in most limestones support cementation under burial and/or meteoric conditions [51,103,110]. According to Adelabu et al. [51], the positive relationship between $\delta^{13}C$ and $\delta^{18}O$ values in the Paleocene–Eocene Ewekoro limestones may indicate diagenetic alteration [104,106]. When freshwater

input is limited and seawater salinity increases, the $\delta^{18}O$ and $\delta^{13}C$ values of sediments tend to increase [111]. In contrast, $\delta^{18}O$ and $\delta^{13}C$ values of minerals may decrease during diagenesis due to mineral phase transformations. Meanwhile, because $\delta^{18}O$ and $\delta^{13}C$ are transferred from minerals to pore waters, the isotopic composition of pore fluids becomes enriched. Consequently, following facies alteration, minerals commonly exhibit depleted $\delta^{18}O$ and $\delta^{13}C$ values [112].

The $\delta^{18}O$ values of the carbonate rocks from the Besni and Garzan formations range from −2.82 to −6.69‰ PDB (mean: −5.09‰ PDB) and from −3.65 to −5.96‰ PDB (mean: −4.71‰ PDB), respectively. The $\delta^{13}C$ values vary between −0.83 and +3.23‰ PDB (mean: +1.37‰ PDB) for the Besni Formation and between +0.89 and +3.39‰ PDB (mean: +1.91‰ PDB) for the Garzan Formation (Table 7). The isotopic compositions of carbonate rocks from both formations are comparable, characterized by negative $\delta^{18}O$ values and predominantly positive $\delta^{13}C$ values (with only two samples from the Besni Formation showing negative $\delta^{13}C$ values). The positive $\delta^{13}C$ values suggest that the carbonate rocks were deposited in a shallow marine environment.

The relationship between $MgCO_3$ content and $\delta^{18}O$ values in the studied carbonates indicates that $\delta^{18}O$ values become depleted with decreasing $MgCO_3$ content (Figure 15F). The calculated temperature (T, °C) for the carbonate rocks shows that $\delta^{18}O$ values decrease (become more negative) with increasing temperature. These negative $\delta^{18}O$ values may also reflect a decrease in salinity associated with increasing temperature [109]. However, because these isotopic values likely incorporate varying degrees of post-depositional overprinting (such as burial diagenesis, cementation, or recrystallization), the calculated temperatures must be explicitly treated as apparent estimates rather than pristine reconstructions of Maastrichtian seawater temperatures. Nonetheless, the general isotopic trends remain useful as a preliminary regional framework, and the stability of $\delta^{13}C$ values relative to temperature variations suggests that the carbon isotope signal was less susceptible to temperature-driven fluid alterations compared to oxygen.

The Z value of carbonate rocks is widely used to determine their origin (marine or freshwater) [49]. Cuna et al. [50] reported that the Upper Paleocene–Lower Eocene Rona limestones exhibit Z values below 120 (106.14–116.22), reflecting a freshwater depositional environment. They also indicated that the average $\delta^{13}C$ composition of these limestones (−4.96‰) is consistent with the values reported for freshwater carbonates of the Tertiary period. Adelabu et al. [53] calculated Z values ranging from 123 to 131 for Paleocene–Eocene Ewekoro limestone samples and suggested that these rocks are of marine origin. In the present study, Z values of carbonate rocks from both formations range from 122 to 132 (average: 128). These results indicate that the carbonate rocks of the Besni and Garzan formations are of marine origin (Table 7).

6. Conclusions

The main findings are summarized as follows:

The carbonate rocks of the Besni Formation were classified based on their components as sandy limestone, packstone, grainstone, wackestone and dolomitic limestone facies. The carbonate rocks of the Garzan Formation were classified as packstone facies according to their textural characteristics and components.

The calculated formation temperatures of the carbonate rocks average 41 °C (range: 34–50 °C) for the Besni Formation and 39 °C (range: 33–46 °C) for the Garzan Formation. However, because these values likely incorporate varying degrees of post-depositional overprinting (such as burial diagenesis, cementation, and recrystallization), they must be explicitly treated as apparent estimates rather than pristine reconstructions of Maastrichtian seawater temperatures or used as direct evidence of climatic warming.

The REE patterns of the carbonate rocks from the Besni and Garzan formations show depletion relative to PAAS-normalized values. In addition, the carbonate rocks exhibit positive Ce and Eu anomalies. Geochemical data from the Garzan and Besni formations indicate that Ce/Ce values* (1.12–1.19 and 0.58–1.49, respectively) plot close to unity, where positive correlations between ΣREE and detrital indicators (SiO_2, Al_2O_3 and Fe) confirm significant detrital contamination. Due to many REE concentrations residing near analytical detection limits, these data fail to support a robust redox proxy interpretation, rendering the observed Ce anomalies inconclusive. Furthermore, the combination of low ΣREE and fossil assemblages typical of an open, shallow-marine platform precludes the existence of persistent anoxic bottom waters during deposition. Finally, while positive Eu anomalies are present, current data remain insufficient to definitively discriminate whether they reflect detrital feldspar, diagenetic processes, or hydrothermal inputs.

When the lithological and petrographic characteristics, major oxide compositions, trace element and REE contents, calculated temperatures, and $\delta^{18}O$ and $\delta^{13}C$ isotopic compositions of the carbonate rocks from the Besni and Garzan formations are evaluated, both formations exhibit similar characteristics and comparable geochemical signatures. These data suggest that the carbonate rocks were deposited in a shallow marine environment. However, given the limited and uneven sampling resolution between the two formations, these comparative geochemical trends should be treated as preliminary rather than a definitive regional framework.

The Besni Formation is characterized by abundant larger benthic foraminifera, including *Orbitoides*, *Omphalocyclus*, *Siderolites*, and *Loftusia*, associated predominantly with packstone and grainstone facies, indicating relatively high-energy shallow-marine depositional conditions. In contrast, the Garzan Formation is characterized by porcelaneous, microgranular, and agglutinated benthic foraminifera associated with dasycladalean algae and predominantly packstone facies, suggesting a relatively protected, lower-energy shallow-marine environment. Despite their stratigraphic equivalence and broadly comparable geochemical characteristics, the differences in foraminiferal assemblages and carbonate microfacies indicate variations in depositional energy between the investigated sections of the two formations.

From a broader palaeogeographic perspective, the Besni and Garzan formations provide an important record of Maastrichtian carbonate-platform evolution along the northernmost sector of the Arabian Plate. While the uneven sampling density constrains the spatial scalability of our findings, their integrated petrographic, palaeontological, and geochemical characteristics provide preliminary insights for regional reconstructions of carbonate-platform evolution immediately prior to the latest Maastrichtian environmental changes recorded elsewhere across the eastern Neo-Tethyan margin.

Author Contributions: Conceptualization, D.S.; methodology, D.S. and S.D.; formal analysis, D.S., S.D., N.Ö.-E. and İ.Ö.Y.; investigation, D.S., S.D. and N.Ö.-E.; writing—original draft preparation, D.S. and S.D.; writing—review and editing, D.S., S.D., N.Ö.-E. and İ.Ö.Y.; visualization, D.S. and S.D.; supervision, N.Ö.-E. and İ.Ö.Y.; project administration, D.S. All authors have read and agreed to the published version of the manuscript.

Funding: This research was funded by Batman University Scientific Research Projects Coordination Unit (BAP), Türkiye, under Project No. BTÜBAP-2019-MMF-01.

Data Availability Statement: All data are included in the manuscript.

Acknowledgments: The authors would like to thank Muhittin Görmüş for his valuable support and contributions to this study. The authors gratefully acknowledge the Editor and the three anonymous reviewers for their constructive and insightful comments, which significantly improved the quality and clarity of this manuscript.

Conflicts of Interest: The authors declare no conflicts of interest.

Abbreviations

The following abbreviations are used in this manuscript:

ΣHREE	Heavy rare earth element
ΣLREE	Light rare earth element
REE	Rare earth element
ICP-MS	Inductively coupled plasma mass spectrometry
VPDB	Vienna Pee Dee Belemnite
PAAS	Post-Archean Australian Shale
K/Pg	Cretaceous–Paleogene boundary
LBF	Larger benthic foraminiferal

References

1. Perinçek, D.; Duran, O.; Bozdoğan, N.; Çoruh, T. Stratigraphy and paleogeographical evolution of the autochthonous sedimentary rocks in the SE Turkey. In *Ozan Sungurlu Symposium Proceedings*; Ozan Sungurlu Vakfı: Ankara, Türkiye, 1991; pp. 274–305.
2. Sinanoğlu, D.; Benedetti, A.; Özgen-Erdem, N. Danian (SBZ2) Larger Foraminifera from the Becirman Formation (Southeastern Turkey) As Evidence of Rotaliids Diversity in Lower Paleocene Shallow-water Environments. *Riv. Ital. Paleontol. Stratigr.* **2022**, *128*, 431–452. [CrossRef] [PubMed]
3. Sinanoğlu, D.; Özgen-Erdem, N.; Sarı, B. Foraminifera from the Maastrichtian Garzan and Lower Germav formations of theArabian Platform (Batman, SE Turkey). *Micropaleontology* **2020**, *66*, 425–440. [CrossRef]
4. Tolun, N. *Besni, Adıyaman, Samsat Arası Bölgelerinin Jeolojik Etüdü*; Derleme No: 2251, 51s, Unpublished Report; MTA: Ankara, Türkiye, 1955.
5. Bolgi, T. *AR/TPI/645, 662, 663, 665 Ruhsat Nolu Adıyaman Sahalarının Jeolojik Etüdü*; Rapor No. 325; TPAO Arama Grubu: Ankara, Türkiye, 1964; 19p.
6. Perinçek, D. *Çelikhan-Sincik-Koçali (Adıyaman Ili) Alanının Jeolojik Incelenmesi*; Rapor No. 1394; TPAO Arama Grubu: Ankara, Türkiye, 1977; 30p.
7. Görür, N.; Akkök, R. *Adıyaman Bölgesinde Mardin Formasyonunun Fasiyes Analizi, Diyajenezi ve Hazne Kaya Niteliği*; Rapor No. 1633; TPAO Arama Grubu: Ankara, Türkiye, 1982; 83p.
8. Meriç, E.; Oktay, F.Y.; Özer, S. Besni Formasyonu'nun Alidamı (Kahta-Adıyaman) kuzeybatısındaki stratigrafikgelişimi ile ilgili yeni gözlemler. *Jeol. Mühendisliği* **1985**, *25*, 51–54.
9. Köylüoğlu, M. *Güneydoğu Anadolu Otokton Birimlerinin Kronostratigrafi, Mikrofasiyes ve Mikrofosilleri*; No. 9; TPAO Araştırma Merkezi: Eğitim Yayınları, 1986; 53p.
10. Perinçek, D.; Günay, Y.; Kozlu, H. Doğu ve Güneydoğu Anadolu bölgesindeki yanal atımlı faylar ile ilgili yeni gözlemler. In *Türkiye 7. Petrol Kongresi*; TPJD: Ankara, Türkiye, 1987; pp. 89–103.
11. Güven, A.; Dinçer, A.; Tuna, M.E.; Tezcan, Ü.Ş.; Çoruh, T. *Güneydoğu Anadolu'da Mardin ve Midyat Grupları Arasında yer Alan Birimlerin Stratigrafisi (Ön Rapor)*; Rapor No. 2414; TPAO Arama Grubu: Ankara, Türkiye, 1988; 154p.
12. Çelikdemir, E.; Dülger, S. *Güneydoğu Anadolu'da Mardin Grubu Karbonatlarının Stratigrafisi, Sedimantolojisi ve Rezervuar Özellikleri*; Rapor No. 2665; TPAO Arama Grubu: Ankara, Türkiye, 1990; 93p.
13. Güven, A.; Dinçer, A.; Tuna, E.M.; Çoruh, T. Stratigraphic evolution of the Campanian-Paleocene autochthonous succession of the Southeast Anatolia. In *Ozan Sungurlu Symposium Proceedings*; Ozan Sungurlu Vakfı: Ankara, Türkiye, 1991; pp. 238–261.
14. Duran, O.; Yılmaz, E. *Güneydoğu Anadolu Bölgesi Otokton ve Allokton Birimler Stratigrafi Adlama Sözlüğü (Lexicon)*; Eğitim Yayınları No. 31; TPAO Genel Müdürlüğü: Ankara, Türkiye, 1997; pp. 1–460.
15. Günay, Y. *Güneydoğu Anadolu'nun Jeolojisi-Stratigrafisi*; Rapor No. 3939, 37 s; TPAO Arama Grubu Başkanlığı: Ankara, Türkiye, 1998.
16. Meriç, E.; Görmüs, M. The genus Loftusia. *Micropaleontology* **2001**, *47*, 1–71.
17. Mülayim, O.; Yilmaz, I.O.; Ferré, B. Roveacrinid microfacial assemblages (Roveacrinida, Crinoidea) from the Lower-Middle Cenomanian of the Adıyaman area (SE Turkey). *Arab. J. Geosci.* **2018**, *11*, 545. [CrossRef]
18. Mülayim, O.; Yilmaz, O.I.; Sarı, B.; Tasli, K.; Wagreich, M. Cenomanian–Turonian drowning of the Arabian Carbonate Platform, the İnişdere section, Adıyaman, SE Turkey. In *Special Publications*; The Geological Society of London: London, UK, 2020; Volume 498, pp. 189–210.
19. Sinanoğlu, D. Systematic and biostratigraphic evaluation of the Late Cretaceous benthic foraminiferal assemblages of southeastern Batman. *Bull. Miner. Res. Explor.* **2021**, *165*, 267–293. [CrossRef]

20. Siyako, M.; Bahtiyar, İ.; Özdoğan, T.; Açıkbaş, İ.; Kaya, Ö.Ç. *Batman Çevresinde Mostra Veren Birimlerin Stratigrafisi*; Rapor No. 5463, Unpublished Report; TPAO Araştırma Merkezi: Ankara, Türkiye, 2013; 154p.
21. Siyako, M.; Şeker, H.; Bahtiyar, İ.; Özdemir, İ.; Kılınç, S.F.; Arslan, D.; Karaçay, A.; Özsoy, S.; Ve İşdiken, B. *Batman, Beşiri, Kurtalan, Raman ve Gercüş Civarının Jeolojisi ve Hidrokarbon Olanakları*; Rapor No. 5546, Unpublished Report; TPAO Arama Dairesi Başkanlığı Arşivi: Ankara, Türkiye, 2015; p. 132.
22. Yıldırım, N.; Çetiner, L. *Adıyaman-Merkez-Koçali (Ar: 200804095) Bakır-Çinko-Altın Sahası Buluculuk Talebine Esas Maden Jeolojisi ve Rezerv Raporu*; Arşiv No: 5543, Unpublished Report; Maden Etüt Arama Dairesi Arşivi: Ankara, Türkiye, 2013.
23. Krummenacher, R.; Periam, C.E. *Geological Studies in the Amanos Mountains with Some Regional Consideration (Report No: GRT.11)*; Unpublished Report; N.V. Turkse Shell (Petrol İşleri Genel Müdürlüğü Teknik Arşivi): Şişli, Istanbul, 1958.
24. İlker, S., VI. *Bölge Adıyaman Kuzey ve Kuzeydoğusundaki Sahalar Hakkında Jeolojik Rapor*; Rapor No. 981, Unpublished Report; TPAO Arama Grubu: Ankara, Türkiye, 1972; 27p.
25. Sungurlu, O., VI. *Bölge Gölbaşı-Gerger Arasındaki Sahanın Jeolojisi*; Rapor No: 802, Unpublished Report; TPAO Arama Grubu: Ankara, Türkiye, 1973; 30p.
26. Sungurlu, O., VI. *Bölge Kuzey Sahalarının Jeolojisi*; Rapor No. 871; TPAO Arama Grubu: Ankara, Türkiye, 1974; 32p.
27. Erdoğan, T. *Gölbaşı Civarının Jeolojisi*; Rapor No.929; TPAO Arama Grubu: Ankara, Türkiye, 1975; 17p.
28. Yalçın, N. *Kahramanmaraş-Gaziantep Arasındaki Allokton Birimlerin Ayırtlanması ve Ilişkileri*; Rapor No. 1249; TPAO Arama Grubu: Ankara, Türkiye, 1978; 68p.
29. Meriç, E. Güneydoğu Türkiye'de Sinan formasyonu alt üyesi ve Besni formasyonunun fauna özellikleri. *TJK Bülteni* **1978**, *21*, 95–96.
30. Günay, Y. *Amonos Dağları'nın Jeolojisi ve Karasu-Hatay Grabeninin Petrololanakları*; Rapor No. 1954; TPAO Arama Grubu: Ankara, Türkiye, 1984; 98p.
31. Meriç, E.; Oktay, F.Y.; Toker, V.; Tanseli, İ.; Duru, M. Adıyaman yöresi Üst Kretase-Eosen istifinin sedimanter jeolojisi ve biyostratigrafisi (foraminifer, nanoplankton, ostracod). *TJK Bülteni* **1987**, *30*, 19–32.
32. Çoruh, T. *Adıyaman Civarında (XI. Bölge Kuzeybatısı ve XII. Bölge) Yüzeyleyen Kampaniyen-Tanesiyen Istifinin Biyostratigrafisi ve Paleocoğrafik Evrimi*; Rapor No. 1656; TPAO Araştırma Merkezi: Ankara, Türkiye, 1991; 101p.
33. Sarıdaş, B. *Cendere Sahası ve Nemrut Dağı Dolayının Jeolojisi (Rezervuar Çalışması)*; Arşiv No. 2826, Unpublished Report; TPAO Arama Grubu: Ankara, Türkiye, 1991; p. 23.
34. Bryant, G.F. *Stratigraphic Report of the Penbeğli-Tutköy Area, Petroleum District VI, Southeast Turkey (American Overseas Petroleum (AMOSEAS) Report)*; Rapor No. 12 (TPAO Arama Grubu, Rapor No. 647), Kutu No. 323, Unpublished Report; Petrol İşleri Genel Müdürlüğü Teknik Arşivi: Ankara, Türkiye, 1960; 27p.
35. Saltık, O.; Saka, K. *Besni Tip Stratigrafi Kesiti*; Arşiv No. 4312; TPAO Arama Grubu: Ankara, Türkiye, 1971; 59p.
36. Tuna, D., VI. *Bölge Litostratigrafı Birimleri Adlamasının Açıklayıcı Raporu*; Rapor No: 813, 131s, Unpublished Report; TPAOArama Grubu: Ankara, Türkiye, 1973.
37. Akça, L. *Adıyaman Tut-İnişdere Dolayı Harita Revizyon Çalışması*; Unpublished Report; TPAO (Türkiye Petrolleri Anonim Ortaklığı) Arama Dairesi Harita Arşivi: Ankara, Türkiye, 1991.
38. Günay, Y.; Sarıtaş, B. *Amanos Dağlarında Cudi-Mardin Grubu Karbonatları ve Üst Kretase-Eosen Yaşlı Istifin Konumu (Rapor No: 2021)*; Unpublished Report; Türkiye Petrolleri Anonim Ortaklığı (TPAO) Arama Dairesi: Ankara, Türkiye, 1991.
39. Kellogg, H.E. *Stratigraphic Report, Bitlis Siirt Area, Petroleum District V, Southeast Turkey*; Rapor No. 2; Petrol İşleri Genel Müdürlüğü Teknik Arşivi: Ankara, Türkiye, 1960; 25p.
40. Salem, R.; Eren, A.; Özbahçeci, H.; Araç, M.; Öncü, H.; İşbilir, M.; Üngör, A.; Biçer, Z.; Yılmaz, Z.; Yılmaz, E. *Geologic and Hydrocarbon Evaluation of Maastrichtian Sediments in Central District X, Southeast Turkey*; Rapor No. 2202; TPAO Arama Grubu: Ankara, Türkiye, 1986; 53p.
41. Özer, S.; Karım, K.H.; Khazaei, A.R. Zagros kuşağı boyunca (Türkiye KD Irak GB İran) Kampaniyen Maastrihtiyen istifleri: Stratigrafi, depolanma ortamları ve paleocoğrafya. In *Türkiye Jeoloji Kurultayı, Abstracts Book*; TMMOB Jeoloji Mühendisleri Odası: Ankara, Türkiye, 2012; 94p.
42. Dunham, R.J. Classification of carbonate rocks according to depositional texture. In *Classification of Carbonate Rocks*; Ham, W.E., Ed.; AAPG: Tulsa, OK, USA, 1962; pp. 108–121.
43. McLennan, S.M. Rare earth elements in sedimentary rocks: Influence of provenance and sedimentary processes. In *Geochemistry and Mineralogy of Rare Earth Elements*; Lipin, B.R., McKay, G.A., Eds.; Mineralogical Society of America: Chantilly, VA, USA, 1989; pp. 169–200.
44. Lawrence, M.G.; Greig, A.; Collerson, K.D.; Kamber, B.S. Rare earth element and yttrium variability in South East Queensland waterways. *Aquat. Geochem.* **2006**, *12*, 39–72. [CrossRef]
45. Taylor, S.R.; McLennan, S.M. *The Continental Crust: Its Composition and Evolution*; Blackwell: Oxford, UK, 1985; p. 312.
46. Epstein, S.; Mayeda, T.K. Variations of the $^{18}O/^{16}O$ ratio in natural waters. *Geochim. Cosmochim. Acta* **1953**, *4*, 213–224.

47. Craig, H. Standard for reporting concentrations of deuterium and oxygen-18 in natural waters. *Science* **1961**, *133*, 1833–1834. [CrossRef] [PubMed]
48. Hayes, P.D.; Grossman, E.L. Oxygen isotopes in meteoric calcite cements as indicators of continental paleoclimate. *Geology* **1991**, *19*, 441–444. [CrossRef]
49. Keith, M.L.; Weber, Y.N. Carbon and oxygen isotopic composition of selected limestone and fossils. *Geochim. Cosmochim. Acta* **1964**, *28*, 1787–1816. [CrossRef]
50. Cuna, S.; Pop, D.; Hosu, A. Carbon and Oxygen Isotope Ratios in Rona Limestone, Romania. *Stud. Univ. Babeş-Bolyai Geol.* **2001**, *46*, 139–151. [CrossRef]
51. Adelabu, I.O.; Opeloye, S.A.; Oluwajana, O.A. Petrography and geochemistry of Paleocene-Eocene (Ewekoro) limestone, eastern Benin basin, Nigeria: Implications on depositional environment and post-depositional overprint. *Heliyon* **2021**, *7*, e08579. [CrossRef] [PubMed]
52. Li, S.; Sanjuan, J.; Wang, Q.; Zhang, H.; Wan, X. Response of the lacustrine flora in East Asia to global climate changes across the K/Pg boundary. *Glob. Planet. Change* **2021**, *197*, 103400. [CrossRef]
53. Keller, G.; Punekar, J.; Mateo, P. Upheavals during the Late Maastrichtian: Volcanism, climate and faunal events preceding the end-Cretaceous mass extinction. *Palaeogeogr. Palaeoclimatol. Palaeoecol.* **2016**, *441*, 137–151. [CrossRef]
54. Hottinger, L. Shallow benthic foraminiferal assemblages as signals for depth of their deposition and their limitations. *Société Géologique Fr. Bull.* **1997**, *168*, 491–505.
55. BouDagher-Fadel, M.K. *Evolution and Geological Significance of Larger Benthic Foraminifera*; Elsevier: Amsterdam, Netherlands, 2008; 714p.
56. Burchette, T.P.; Wright, V.P. Carbonate ramp depositional systems. *Sediment. Geol.* **1992**, *79*, 3–57. [CrossRef]
57. Flügel, E. *Microfacies of Carbonate Rocks: Analysis, Interpretation and Application*, 2nd ed.; Springer: Berlin/Heidelberg, Germany, 2010.
58. Ghanbarloo, H.; Safari, A.; Vaziri-Moghaddam, H. Biostratigraphy and Sequence Stratigraphy of the Tarbur Formation (Maastrichtian) from Iranian Zagros Foreland Basin, Southwest of Iran. *Acta Geol. Sin. (Engl. Ed.)* **2022**, *96*, 147–166. [CrossRef]
59. Hottinger, L. The depth-depending ornamentation in larger foraminifera. *Palaeogeogr. Palaeoclimatol. Palaeoecol.* **2006**, *242*, 188–205.
60. Schlager, W. *Carbonate Sedimentology and Sequence Stratigraphy*; SEPM Concepts in Sedimentology and Paleontology, No. 8; Society for Sedimentary Geology (SEPM): Tulsa, OK, USA, 2005; 200p.
61. Arefifard, S.; Davydov, V.I. Petrography and Geochemistry of Permian Strata in Tabas and Kalmard Regions, Eastern-Central Iran. *Geophys. Res. Abstr.* **2005**, *7*, 00484.
62. Brand, U.; Veizer, J. Chemical diagenesis of multicomponent carbonate system-2: Stable isotopes. *Jour. Sedim. Petrol.* **1981**, *51*, 987–997. [CrossRef]
63. Rao, C.P. Geochemistry of the Gordon Limestone (Ordovician), Mole Creek, Tasmania. *Aust. J. Earth Sci.* **1989**, *36*, 65–71. [CrossRef]
64. Reimer, T.O. Diagenetic reactions in early precambrian gray wackes of the Barberton Mountain land (South Africa). *Sediment. Geol.* **1972**, *7*, 263–282. [CrossRef]
65. Degens, E.T.; Williams, E.G.; Keith, M.L. Environmental studies of Carboniferous sediments. Part I: Geochemical criteria for differentiating marine and fresh-water shales. *Bull. Amer. Assoc. Petrol. Geol.* **1957**, *41*, 2427–2455. [CrossRef]
66. Friedman, G.M. Terminology of crystallization textures and fabrics in sedimentary rocks. *J. Sediment. Petrol.* **1965**, *35*, 643–655. [CrossRef]
67. Mirza, T.A.; Karim, K.H.; Ridha, S.M.; Fatah, C.M. Major, trace, rare earth element, and stable isotope analyses of the Triassic carbonates along the northeastern Arabian Plate margin: A key to understanding paleotectonics and paleoenvironment of the Avroman (Biston) limestone formation from Kurdistan region, northeastern Iraq. *Carbonates Evaporites* **2021**, *36*, 66. [CrossRef]
68. Schieber, J. Redistribution of rare-earth elements during diagenesis of carbonate rocks from the Mid-Proterozoic Newland formation, Montana, USA. *Chem. Geol.* **1988**, *69*, 111–126. [CrossRef]
69. Armstrong-Altrin, J.S.; Nagarajan, R.; Madhavaraju, J.; Rosales-Hoz, L.; Lee, Y.I.; Balaram, V.; Cruz-Martinez, A.; Avila-Ramirez, G. Geochemistry of the Jurassic and upper cretaceous shales from the Molango region, Hidalgo, eastern Mexico: Implications for source-area weathering, provenance, and tectonic setting. *Compt. Rendus Geosci.* **2013**, *345*, 185–202. [CrossRef]
70. Tostevin, R.; Shields, G.A.; Tarbuck, G.M.; He, T.; Clarkson, M.O.; Wood, R.A. Effective use of cerium anomalies as a redox proxy in carbonate-dominated marine settings. *Chem. Geol.* **2016**, *438*, 146–162. [CrossRef]
71. Shields, G.A.; Webb, G.E. Has the REE composition of seawater changed over geological time? *Chem. Geol.* **2004**, *204*, 103–107. [CrossRef]
72. Elderfield, H.; Greaves, M. The rare earth elements in seawater. *Nature* **1982**, *296*, 214–219. [CrossRef]
73. Shields, G.; Stille, P. Diagenetic Constraints on the Use of Cerium Anomalies as Palaeoseawater Redox Proxies: An Isotopic and REE Study of Cambrian Phosphorites. *Chem. Geol.* **2001**, *175*, 29–48. [CrossRef]

74. Peckmann, J.; Thiel, V.; Michaelis, W.; Clari, P.; Gaillard, C.; Martire, L.; Reitner, J. Cold seep deposits of Beauvoisin (Oxfordian; southeastern France) and Marmorito (Miocene; northern Italy): Microbially induced authigenic carbonates. *Int. J. Earth Sci.* **1999**, *88*, 60–75. [CrossRef]
75. Qing, H. Petrology and geochemistry of early-stage, fine-and mediumcrystalline dolomites in the Middle Devonian Presqu'ile Barrier at Pine Point, Canada. *Sedimentology* **1998**, *45*, 433–446. [CrossRef]
76. Piepgras, D.J.; Jacobsen, S.B. The behaviour of rare earth elements in seawater: Precise determination of variations in the North Pacifc water column. *Geochem. Cosmochem. Acta* **1992**, *56*, 1851–1862. [CrossRef]
77. Murray, R.W.; Ten Brink, M.R.B.; Gerlach, D.C.; Russ, G.P.; Jones, D.L. Rare earth, major, and trace elements in chert from the Franciscan complex and monterey Group, California: Assessing REE sources to fine-grained marine sediments. *Geochem. Cosmochem. Acta* **1991**, *55*, 1875–1895. [CrossRef]
78. Madhavaraju, J.; Lee, Y.I. Geochemistry of the Dalmiapuram Formation of the Uttatur Group (Early Cretaceous), Cauvery Basin, southeastern India: Implications on provenance and paleoredox conditions. *Rev. Mex. Cienc. Geológicas* **2009**, *26*, 380–394.
79. Madhavaraju, J.; Gonzalez-Leon, C.M. Depositional conditions and source of rare earth elements in carbonate strata of the Aptian-Albian Mural formation, Pitaycachi section, northeastern Sonora, Mexico. *Rev. Mex. Cienc. Geológicas* **2012**, *29*, 478–491. [CrossRef]
80. Nothdurft, L.D.; Webb, G.E.; Kamber, B.S.R. Rare earth element geochemistry of Late Devonian reefal carbonates, Canning Basin, Western Australia: Confirmation of a seawater REE proxy in ancient limestones. *Geochem. Cosmochem. Acta* **2004**, *68*, 263–283. [CrossRef]
81. Olivier, N.; Boyet, M. Rare earth and trace elements of microbialites in Upper Jurassic coral and sponge-microbialite reefs. *Chem. Geol.* **2006**, *230*, 105–123. [CrossRef]
82. Nath, B.N.; Bau, M.; Ramalingeswara Rao, B.; Rao, C.M. Trace and rare earth elemental variation in Arabian Sea sediments through a transect across the oxygen minimum zone. *Geochim. Cosmochim. Acta* **1997**, *61*, 2375–2388. [CrossRef]
83. Madhavaraju, J.; Ramasamy, S. Rare earth elements in limestones of Kallankurichchi Formation of Ariyalur Group, Tiruchirapalli Cretaceous, Tamil Nadu. *J. Geol. Soc. India* **1999**, *54*, 291–301. [CrossRef]
84. Madhavaraju, J.; González-León, C.M.; Lee, Y.I.; Armstrong-Altrin, J.S.; Reyes-Campero, L.M. Geochemistry of the Mural Formation (Aptian-Albian) of the Bisbee Group, Northern Sonora, Mexico. *Cretac. Res.* **2010**, *31*, 400–414. [CrossRef]
85. Haley, B.A.; Klinkhammer, G.P.; McManus, J. Rare earth elements in pore waters of marine sediments. *Geochim. Cosmochim. Acta* **2004**, *68*, 1265–1279. [CrossRef]
86. Oliveri, E.; Neri, R.; Bellanca, A.; Riding, R. Carbonate stromatolites from a Messinian hypersaline setting in the Caltanissetta Basin, Sicily: Petrographic evidence of microbial activity and related stable isotope and rare earth element signatures. *Sedimentology* **2010**, *57*, 142–161. [CrossRef]
87. Franchi, F.; Turetta, C.; Cavalazzi, B.; Corami, F.; Barbieri, R. Trace elements and REE geochemistry of Middle Devonian carbonate mounds (Maïder Basin, Eastern Anti-Atlas, Morocco): Implications for early diagenetic processes. *Sediment. Geol.* **2016**, *343*, 56–71. [CrossRef]
88. Parsapoor, A.; Khalili, M.; Mackizadeh, M.A. The behaviour of trace and rare earth elements (REE) during hydrothermal alteration in the Rangan area (Central Iran). *J. Asian Earth Sci.* **2009**, *34*, 123–134. [CrossRef]
89. Bau, M.; Balan, S.; Schmidt, K.; Koschinsky, A. Rare earth elements in mussel shells of the Mytilidae family as tracers for hidden and fossil high-temperature hydrothermal systems. *Earth Planet. Sci. Lett.* **2010**, *299*, 310–316. [CrossRef]
90. Piper, D.Z. Rare earth elements in the sedimentary cycle, a summary. *Chem. Geol.* **1974**, *14*, 285–304. [CrossRef]
91. Madhavaraju, J.; Löser, H.; Scott, R.W.; Sandeep, S.; Sial, A.N.; Ramasamy, S. Petrography, geochemistry and stable isotopes of carbonate rocks, Lower Cretaceous Alisitos Formation, Los Torotes section, Baja California, Mexico. *Rev. Mex. Cienc. Geológicas* **2017**, *34*, 63–77. [CrossRef]
92. Michard, A.; Albarède, F.; Michard, G.; Minster, J.F.; Charlou, J.L. Rare earth elements and uranium in high temperature solutions from East-Pacific rise hydrothermal vent field (13°N). *Nature* **1983**, *303*, 795–797. [CrossRef]
93. Klinkhammer, G.; Elderfield, H.; Hudson, A. Rare earth elements in seawater near hydrothermal vents. *Nature* **1983**, *305*, 185–188. [CrossRef]
94. German, C.R.; Mills, R.; Blusztajn, J.; Fleer, P.A.; Bacon, M.P.; Higgs, N.C.; Elderfield, H.; Thomson, J. A geochemical study of metalliferous sediment from the TAG hydrothermal mound, 26°08′ N, Mid-Atlantic ridge. *J. Geophys. Res.* **1993**, *98*, 9683–9692. [CrossRef]
95. Sherrell, R.M.; Field, M.P.; Ravizza, G. Uptake and fractionation of rare earth elements on hydrothermal plume particles at 9°45′N, East Pacific Rise. *Geochim. Cosmochim. Acta* **1999**, *63*, 1709–1722. [CrossRef]
96. MacRae, N.D.; Nesbitt, H.W.; Kronberg, B.I. Development of a positive Eu anomaly during diagenesis. *Earth Planet. Sci. Lett.* **1992**, *109*, 585–591. [CrossRef]

97. Madhavaraju, J.; Löser, H.; Lee, Y.I.; Lozano-SantaCruz, R.; Pi-Puig, T. Geochemistry of Lower Cretaceous limestones of the Alisitos Formation, Baja California, Mexico: Implications for REE source and paleo-redox conditions. *J. S. Am. Earth Sci.* **2016**, *66*, 149–165. [CrossRef]
98. Kurian, S.; Nath, B.N.; Ramasamy, V.; Naman, D.; Gnaneshwar, R.; Kamesh Raju, K.A.; Selvaraj, K.; Chen, C.T.A. Possible, detrital, diagenetic and hydrothermal sources for Holocene sediments of the Andaman backarc basin. *Mar. Geol.* **2008**, *247*, 178–193. [CrossRef]
99. Shao, H.; Xu, Y.G.; He, B.; Huang, X.L.; Luo, Z.Y. Petrology and geochemistry of the late-stage acidic volcanic rocks of the Emeishan large igneous province. *Bull. Mineral. Petrol. Geochem.* **2007**, *26*, 350–358.
100. Zhu, D.; Jin, Z.; Hu, W. Hydrothermal recrystallization of the Lower Ordovician dolomite and its significance to reservoir in northern Tarim Basin. *Sci. China Earth Sci.* **2010**, *53*, 368–381. [CrossRef]
101. Tucker, M.E.; Wright, V.P. *Carbonate Sedimentology*; Blackwell Science: Oxford, UK, 1990; 482p.
102. Allan, J.R.; Matthews, R.K. Isotope signatures associated with early meteoric diagenesis. *Sedimentology* **1982**, *29*, 797–817. [CrossRef]
103. Madhavaraju, J.; Lee, Y.I.; González-León, C.M. Diagenetic significance of carbon, oxygen and strontium isotopic compositions in the Aptian-Albian Mural Formation in Cerro Pimas area, northern Sonora, Mexico/Significado diagenético de las composiciones isotópicas de carbono, oxígeno y estroncio en la Formación Mural (Aptiense-Albiense, zona Cerro Pimas, norte de Sonora, México). *J. Iber. Geol.* **2013**, *39*, 73–88.
104. Armstrong-Altrin, J.S.; Madhavaraju, J.; Sial, A.N.; Kasper-Zubillaga, J.J.; Nagarajan, R.; Flores-Castro, K.; Rodríguez, J.L. Petrography and stable isotope geochemistry of the cretaceous El Abra Limestones (Actopan), Mexico: Implication on diagenesis. *J. Geol. Soc. India* **2011**, *77*, 349–359. [CrossRef]
105. Hossain, H.Z.; Sultan-Ul-Islam, M.; Armstrong-Altrin, J.S.; Sial, A.N.; Ahamed, S.; Nowsher, M.N.; Abdullah-Al-Kawsar, M. Stable carbon and oxygen isotopic composition of mio-pliocene bivalve shells and calcareous sediments in nhila anticline, southeast bengal basin, Bangladesh. *J. Life Earth Sci.* **2013**, *8*, 113–117. [CrossRef]
106. Marshall, J. Climatic and oceanographic isotopic signals from the carbonate rock record and their preservation. *Geol. Mag.* **1992**, *129*, 143–160. [CrossRef]
107. Nagarajan, R.; Armstrong-Altrin, J.S.; Sial, A.N.; Nagendra, R.; Ellam, R.M. Carbon, oxygen, and strontium isotope geochemistry of the Proterozoic carbonate rocks, Bhima basin, south India: Implication for diagenesis. *Carpathian J. Earth Environ. Sci.* **2013**, *8*, 25–38.
108. Veizer, J. Chemical Diagenesis of Carbonates: Theory and Application of Trace Element Technique. In *Stable Isotopes in Sedimentary Geology*; Arthur, M.A., Anderson, T.F., Kaplan, I.R., Veizer, J., Land, L.S., Eds.; Society of Economic Paleontologists and Mineralogists Short Course; SEPM (Society for Sedimentary Geology): Claremore, OK, USA, 1983; Volume 10, pp. 3-1–3-100.
109. Hudson, J.D. Stable isotopes and limestone lithification. *J. Geol. Soc.* **1977**, *133*, 637–660. [CrossRef]
110. Armstrong-Altrin, J.S.; Lee, Y.I.; Verma, S.P.; Worden, R.H. Carbon, oxygen, and strontium isotope geochemistry of carbonate rocks of the upper Miocene Kudankulam Formation, southern India: Implications for paleoenvironment and diagenesis. *Geochemistry* **2009**, *69*, 45–60. [CrossRef]
111. Jaffrés, J.B.D.; Shields, G.A.; Wallmann, K. The oxygen isotope evolution of seawater: A critical review of a long-standing controversy and an improved geological water cycle model for the past 3.4 billion years. *Earth-Sci. Rev.* **2007**, *83*, 83–122. [CrossRef]
112. Geske, A.; Zorlu, J.; Richter, D.K.; Buhl, D.; Niedermayr, A.; Immenhauser, A. Impact of diagenesis and low grade metamorphosis on isotope (δ26Mg, δ13C, δ18O and 87Sr/86Sr) and elemental (Ca, Mg, Mn, Fe and Sr) signatures of Triassic sabkha dolomites. *Chem. Geol.* **2012**, *332*, 45–64. [CrossRef]

Disclaimer/Publisher's Note: The statements, opinions and data contained in all publications are solely those of the individual author(s) and contributor(s) and not of MDPI and/or the editor(s). MDPI and/or the editor(s) disclaim responsibility for any injury to people or property resulting from any ideas, methods, instructions or products referred to in the content.